Tracked changes version for review

Contrasts in dissolved, particulate and sedimentary organic carbon from the Kolyma River to the East Siberian Shelf

Dirk Jong[1], Lisa Bröder[1,2], Tommaso Tesi[3], Kirsi Keskitalo[1], Nikita Zimov[4], Anna Davydova[4], Philip Pika[1], Negar Haghipour[2], Timothy Eglinton[2], Jorien Vonk[1]

[1] Department of Earth Sciences, Vrije Universiteit, Amsterdam, the Netherlands
[2] Geological Institute, Swiss Federal Institute of Technology, Zürich, Switzerland
[3] Institute of Polar Sciences, National Research Council, Bologna, Italy
[4] Pacific Geographical Institute, Far East Branch, Russian Academy of Sciences, Northeast Science Station, Cherskiy, Russia

Correspondence to: Dirk Jong (d.j.jong@vu.nl), Jorien Vonk (j.e.vonk@vu.nl)

Abstract. Arctic rivers will be increasingly affected by the hydrological and biogeochemical consequences of thawing permafrost. During transport, permafrost-derived organic carbon (OC) can either accumulate in floodplain and shelf sediments or be degraded into greenhouse gases prior to final burial. Thus, the net impact of permafrost OC on climate will ultimately depend on the interplay of complex processes that occur along the source-to-sink system. Here, we focused on the Kolyma River, the largest watershed completely underlain by continuous permafrost, and marine sediments of the East Siberian Sea as a transect to investigate the fate of permafrost OC along the land-ocean continuum. Three pools of riverine OC were investigated for the Kolyma main stem and five of its tributaries: dissolved OC (DOC), suspended particulate OC (POC), and riverbed sediment OC (SOC) and compared to earlier findings in marine sediments. Carbon isotopes ($\delta^{13}C$, $\Delta^{14}C$), lignin phenol, and lipid biomarker~~s~~ proxies show a contrasting composition and degradation state of these different carbon pools. Dual C isotope source apportionment calculations imply that old permafrost-OC is mostly associated with sediments (SOC; contribution of 68 ± 10%), and less dominant in POC (38 ± 8%), while autochthonous primary production contributes around 44 ± 10% to POC in the main stem and up to 79 ± 11% in tributaries. Biomarker degradation indices suggest that Kolyma DOC is relatively degraded, regardless of its generally young age shown by previous studies. In contrast, SOC shows the lowest $\Delta^{14}C$ ~~signal~~ value (oldest OC), yet relatively fresh compositional signatures. Furthermore, decreasing mineral surface area-normalised OC- and biomarker loadings suggest that SOC is reactive along the land-ocean continuum~~. We found that~~and almost all parameters were subjected to rapid change when moving from freshwater to the marine environment. This suggests that sedimentary dynamics play a crucial role when targeting permafrost-derived OC in aquatic systems and ~~also~~ supports earlier studies highlighting that the land-ocean transition zone is an efficient reactor and a dynamic environment~~, especially in the estuarine environment, supporting the idea that floodplain, delta, and shelf sediments are efficient reactors~~. The prevailing inconsistencies between freshwater and marine research (i.e. targeting predominantly DOC and SOC, respectively) need to be better aligned in order to determine to what degree thawed permafrost OC may be destined for long-term burial, therewith attenuating further global warming. ~~A better understanding of DOC and POC dynamics in Arctic rivers is still necessary, however, this study highlights that sedimentary dynamics play a crucial role when targeting permafrost-derived OC in aquatic systems. Chemical and physical processes (e.g. degradation, sorption)~~are diverse along fluvial marine transects and the ~~transition zone between these two environments, and will determine to what degree thawed permafrost OC may be destined for long-term burial, therewith attenuating further global warming.~~

1 Introduction

Permafrost regions store approximately half of the global soil organic carbon (OC) (Hugelius et al., 2014; Zimov et al., 2006a). Amplified warming of the Arctic, currently three times as fast as the global average (IPCC, 2021), warms permafrost on a global scale (Biskaborn et al., 2019). Permafrost thaw and associated shifts in hydrology (Walvoord and Kurylyk, 2016),

impact regional carbon cycling through the release of organic matter from this previously frozen pool to the fluvial network. In addition, the release of nutrients and sediment leads to a multitude of effects on the biogeochemical properties of inland and coastal waters (Terhaar et al., 2021; Vonk et al., 2015). Furthermore, decomposition of OC from thawing permafrost soils releases greenhouse gases (CO_2, CH_4) into the atmosphere causing further climate warming (Schuur et al., 2015).

Arctic rivers, as rivers in general, serve as integrators of their catchments tracking changes in terrestrial signatures of the transported organic matter at the river mouth, and can therefore be used as indicators for watershed-wide processes such as permafrost thaw or soil remobilization (van Dongen et al., 2008; Wild et al., 2019; Feng et al., 2013). Based on river mouth ~~sampling campaigns~~monitoring, the six largest Arctic rivers are estimated to transport 40 Tg of fluvial OC, of which 34 Tg DOC and 6 Tg POC, into the Arctic Ocean (Holmes et al., 2012; McClelland et al., 2016). These estimates serve as important baseline data for terrestrial carbon export to the Arctic Ocean. However, fluvial OC cycling already occurs in headwater streams, and extends beyond the river mouth to the shelf seas. Inland waterways are known not just to conservatively channel fluvial OC towards the ocean, but also on one hand actively degrade OC into greenhouse gases and on the other hand sequester OC on short- and long timescales (days to millennia) (Cole et al., 2007; Drake et al., 2018). Similarly, breakdown of terrestrial OC in the marine environment (e.g., Alling et al., 2010; Bröder et al., 2018), subsequent ocean acidification (Semiletov et al., 2016) and increase in marine primary production (Terhaar et al., 2021) have been the focus of recent studies. To better assess processing and fate of terrestrial organic matter in aquatic systems, we should regard these environments to be linked in a land-ocean continuum or as a carbon cycle 'without boundaries' (Battin et al., 2009).

For a complete assessment of fluvial OC, one needs to look at three different compartments: dissolved organic carbon (DOC; operationally defined as <0.7 µm), suspended particulate organic carbon (POC; >0.7 µm) and sedimentary organic carbon (SOC). In the six largest Arctic rivers, DOC concentrations are generally higher than those of POC (Holmes et al., 2012; McClelland et al., 2016), however, DOC consists predominantly of recent terrestrial material, while POC is predominantly sourced from deeper soils and permafrost (Wild et al., 2019). The fraction of DOC that is derived from Yedoma permafrost, Pleistocene-aged permafrost deposits rich in OC,~~-~~ along the Kolyma River is rapidly degraded upon thaw (Mann et al., 2015; Rogers et al., 2021; Vonk et al., 2013). In contrast, POC derived from thermal erosion of river banks and coastlines, thermokarst, and other abrupt permafrost thaw features may be less prone to rapid degradation, and transported over longer distances (Keskitalo et al., 2022; Salvadó et al., 2016). Concentrations, fluxes and isotopic signatures of POC in Arctic rivers have been studied in the past decade (McClelland et al., 2016; Wild et al., 2019), including more recent studies on the molecular structure and~~-~~ degradation (e.g, Kolyma river; Bröder et al., 2020; Keskitalo et al., 2022). However, the cycling and degradation of POC during lateral aquatic transport, and especially its interplay with DOC and SOC remains elusive.

To better understand the interaction and exchange of POC with river- and marine sediments, as well as DOC, all these OC pools need to be considered. Yet to date, studies on riverine SOC transport and degradation are limited and contradictory. In the Danube River, SOC concentrations and mineral-specific surface area-normalised biomarker loadings decrease downstream, suggesting significant SOC degradation during fluvial transport (Freymond et al., 2018). On the contrary, Scheingross et al. (2019) found in an experimental setting that particle abrasion and turbulent mixing of POC in the water column has only a limited effect on degradation, and suggests that degradation takes place mostly during floodplain storage of sediment. Repasch et al. (2021) (Rio Bermejo, Argentina) and ~~(~~Hilton et al.~~,~~ (2015) (Mackenzie River, Canada) show that eroded POC is efficiently transported by rivers, and redeposited in floodplains or basins offshore, and suggest that sediment transport time and mineral protection of OC regulate the magnitude and rate of POC degradation. Additionally, processes such as leaching of POC and SOC, and, vice versa, adsorption of DOC to soil or mineral particles influences both the composition and degradability of OC: mineral binding ballasts and slows down degradation of OC (Hemingway et al., 2019; Keil et al., 1994; Keskitalo et al., 2022; Kleber et al., 2021; Vonk et al., 2010b), while leaching of OC to the dissolved phase increases its potential for degradation (Abbott et al., 2014; Mann et al., 2015; Rogers et al., 2021; Vonk et al., 2013). No previous studies,

according to our knowledge, have addressed transport and degradation of SOC in the Kolyma River using riverbed samples upstream from the Kolyma ~~r~~River mouth.

Here we, for the first time in this river system, combine the ~~use an integrated approach, for a combined~~ investigation of three fractions of fluvial OC (dissolved, particulate and sedimentary), ~~fractions of OC~~ along a 250-km long river transect in the lower reaches of the Kolyma River, including five of its tributaries. ~~We apply a variety of bulk analyses (OC%, $\delta^{13}C$, $\Delta^{14}C$, mineral-specific surface area), and use molecular geochemical tracers (long-chain *n*-alkanoic acids, and lignin and cutin-derived products) to untangle, for each fraction, the sources of OC and its degradation state.~~ Furthermore, we connect our fluvial data with published records from~~or~~ a 1000 km-long transect across the East Siberian Sea (ESS) (Tesi et al., 2014; Vonk et al. 2010, 2012; Bröder et al., 2019; Salvadó et al., 2016), We applied~~y~~ a variety of bulk analyses (OC%, $\delta^{13}C$, $\Delta^{14}C$, mineral-specific surface area), and used molecular geochemical tracers (long-chain *n*-alkanoic acids, and lignin and cutin-derived products) to untangle, for each fraction of OC, ~~the~~its sources ~~of OC~~ and the effect of fractionation and degradation~~and its degradation state. to track the changes of each phase (dissolved, particulate and sediment OC) and the effect of fractionation and degradation on the state of terrestrial OC~~ during its ~~aquatic~~ transport via different aquatic (freshwater, marine) and sedimentary ~~over large distances and through different sedimentary~~ (i.e. river, delta, estuary, shelf) ~~and aquatic (freshwater versus marine)~~ environments ~~along~~ of the land-ocean continuum.

2 Methods

2.1 Study area and sample locations

The Kolyma River in Northeast Siberia is the world's largest watershed (653,000 km^2) entirely underlain by continuous permafrost (Holmes et al., 2012). Its discharge follows a distinct seasonal pattern typical for Arctic rivers, with a strong peak during the spring freshet, and lower baseflow in winter. Annual water discharge is 109 ± 7 km^3 (Holmes et al., 2012), and the average annual DOC and POC flux from the Kolyma River to the East Siberian Sea is 818 Gg (10^9 g) and 123 Gg per year, respectively (Holmes et al., 2012; McClelland et al., 2016). In its lower reaches, the river flows roughly northward through lowlands that consist of icy loess-like Yedoma deposits, or Ice complex permafrost deposits (ICD), of Pleistocene age. This Yedoma permafrost has a high OC content (2 – 5%; Zimov et al., 2006b). Most of the Kolyma watershed is covered by boreal forests (taiga) dominated by the Cajanderi larch (*Larix cajanderi Mayr*), and the Kolyma Delta further north is in the tundra biome.

Sampling of the Kolyma River took place from the Northeast Science Station in Cherskiy during summer 2018, from 23 July to 3 August, directly after spring freshet (Figure A1). We covered a 250 km-long transect of the Kolyma River starting at 68.63890 °N 159.12080 °E, where the river passes a ca. 10 km long Yedoma-deposit riverbank exposure (Duvanny Yar, DY) to the delta outflow into the East Siberian Sea, including sampling the lesser-studied western delta branch of the Kolyma River (K1-K6, Fig. 1b, Table 1). In addition to the samples from the Kolyma River main stem, samples were taken from several tributaries with varying catchment sizes. Two of the larger tributaries of the Kolyma were sampled, the Maly Anyuy (MA), and the Bolshoy Anyuy (BA), with a catchment size of 49,800 and 57,300 km^2, respectively, and a smaller tributary, the Panteleikha (PAN; 1,630 km^2), where an algal bloom was observed at the time of sampling (30 July 2018). In addition, two small streams with contrasting characteristics were sampled: i) Y3 (~17 km^2), characterised by a relatively high DOC load and low POC load, representing soil leaching and active layer drainage (Bröder et al., 2020), and ii) a thaw stream at Duvanny Yar (DY TS; <0.1 km^2), characterised by an extremely high POC load, and relatively low DOC load, representing eroding Yedoma permafrost (Vonk et al., 2013). At Duvanny Yar, additional samples were taken from a thawing permafrost headwall, and from the outflow of a thaw stream into the Kolyma River (DY KOL) to characterize the Yedoma permafrost endmember and mixing of the thaw streams with Kolyma waters.

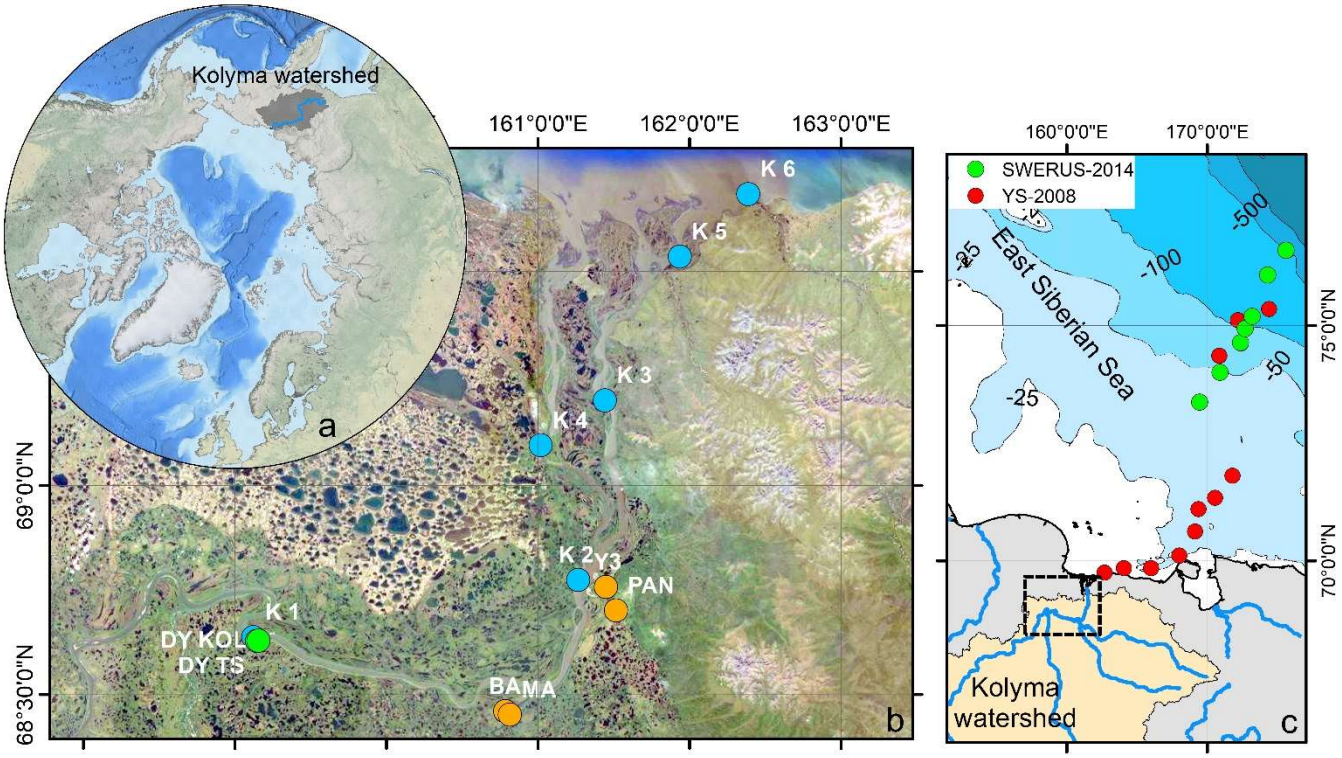

Figure 1. (a) Location of the Kolyma watershed (Made with ArcMap™, Copyright © Esri. All rights reserved.). (b) Kolyma River delta with sample locations. In blue the Kolyma mainstem samples, orange the tributaries (Panteleikha (PAN), Bolshoy and Maly Anyuy (BA and MA), and Y3), green Duvanny Yar (DY). For reference location K 2 is located at the town of Cherskiy. Background image adapted from (Mann et al., 2012). (c) Sample location in the East Siberian Sea following the Kolyma paleoriver-transect, extended to the shelf break. ~~The white box is the location of the Kolyma Delta~~. In red, ~~F~~first 8 locations offshore from South to North: YS34B to YS41 (Vonk et al., 2010a; Tesi et al., 2014); ~~104~~ locations farther offshore from South to North: YS91, YS90/SWE-63, YS88, YS86. In green, south to north: SWE-60, SWE-61~~, YS91, YS90,~~ YS90/SWE-63, SWE-64, ~~YS88,~~ SWE-65, ~~YS86,~~ SWE-66 and SWE-67 (Salvadó et al., 2016; Bröder et al., 2019). The black box shows the location of panel (b).

We compare our samples with the data reported in Bröder et al. (2020), including POC samples from the Kolyma River (sampled at Cherskiy) and the tributary stream Y3, covering the open-water seasons (late May until late September/early October) of 2013 and 2015. These samples were included in the present study to give insight into temporal variations at these locations, in addition to spatial variations along the transect.

Furthermore, this new dataset is compared to published data on surface water DOC and POC, and surface sediments from the East Siberian Sea. The East Siberian Sea is situated between the Laptev Sea and the New Siberian Islands to the west and the Chukchi Sea and Wrangel Island to the east (Fig. 1a). It covers an area of approximately one million square kilometres, and has an average depth of 58 meters. Previous publications (Tesi et al., 2014; Vonk et al. 2010, 2012a) have characterized surface water DOC and POC in the ESS, along with underlying surface sediments, following the paleo river valley of the Kolyma up to 600 km offshore (Fig. 1c). The samples along this transect were collected on 3-5 September 2008, and started ca. 12 km farther offshore than our farthest river transect point (K6). An increase in salinity was measured in surface water moving from K 5 (0.15) to K 6 (2.6) to the first point of the marine transect (YS-34B, 17.8; Vonk et al., 2010). Data from a more recent cruise (between 31 July and 4 August 2014) are used to extend this transect up to 1000 km offshore (Bröder et al., 2019; Salvadó et al., 2016). The ESS around the extended transect is influenced by the Pacific inflow and the Transpolar Drift farther offshore, and the West to East flowing Siberian Coastal Current closer to shore (Stein and Macdonald, 2004; Duradev et al., 2022). The list of ESS station locations and data used in this study can be found in Table A1.

Table 1. Sample locations, description, sampling data, short ID, and the distance of each location to the mouth of the Kolyma River.

Short ID	Location description	Date sampled	Latitude (°)	Longitude (°)	Distance to ocean (km)
Kolyma					
K 1	Before Duvanny Yar	23/07/2018	N 68.63890	E 159.12080	240
K 2	At Cherskiy	31/07/2018	N 68.77598	E 161.26494	110
K 3	Eastern branch	28/07/2018	N 69.20045	E 161.44044	60
K 4	Western branch	31/07/2018	N 69.09501	E 161.01700	60
K 5	Main delta channel	28/07/2018	N 69.53432	E 161.93555	10
K 6	Outflow to ESS	28/07/2018	N 69.67805	E 162.38632	0
Duvanny Yar					
DY TS	Yedoma thaw stream	02/08/2018	N 68.62987	E 159.14470	230
DY KOL	Kolyma directly at thaw stream outflow	23/07/2018	N 68.63060	E 159.15478	230
Tributaries					
BA	Bolshoy Anyui	01/08/2018	N 68.46015	E 160.78267	160
MA	Maly Anyui	01/08/2018	N 68.45193	E 160.81279	160
Y3	Y3	26/07/2018	N 68.75919	E 161.44769	120
PAN	Panteleikha	30/07/2018	N 68.70301	E 161.51472	120

2.2 Sampling and sample processing

2.2.1 Particulate and dissolved organic matter, and solid phase extractions

About 20 L of surface water was collected in LDPE bags (Vitop, Rink GmbH) in the centre of the ~~or the fastest flowing part of the~~ river at each location, except for sample DY KOL, which was sampled at the shore of the Kolyma in the outflow of a thaw stream (Table 1). Within 12 hours after sampling, the collected surface water was filtered through pre-combusted (400 °C, 12 h including temperature ramping) and pre-weighed glass fibre filters (pore size 0.7 µm, Whatman GF/F). Small GF/F filters (diameter 47 mm; glass filtration tower, Wheaton) were used for total suspended particulate matter (SPM), POC concentration, and carbon isotope analyses, whereas large GF/F filters (diameter 90 mm, pore size 0.7 µm, Whatman; custom made, stainless steel filtration tower) were used to collect larger quantities of suspended material for biomarker analysis. Filters were stored and transported frozen (-20°C), and freeze-dried before further analyses.

The filtrate (DOC) was stored in pre-combusted 40 mL amber glass vials, acidified to pH 2 with concentrated HCl, and transported refrigerated (+5 °C) and dark. After subsampling, the remaining filtrate (0.8 to 12.8 L, depending on DOC concentration) was used for the solid phase extraction (SPE) of DOC, following the method of Louchouarn et al. (2000) and Spencer et al. (2010). For this purpose, the filtrate was acidified to pH 2 using concentrated HCl (37%) and 2% of methanol was added to aid extraction efficiency (Spencer et al., 2010). The acidified filtrate was pumped through a pre-rinsed SPE cartridge (60 mL Mega Bond-Elut C18; Agilent) using a peristaltic pump with flexible silicone tubing (Cole-Parmer instrument company). The loaded SPE cartridges were stored and transported refrigerated (+5 °C) and dark. Back at the Vrije Universiteit Amsterdam, the SPE cartridges were extracted by eluting twice with 40 ml of methanol into pre-combusted glass vials, which were subsequently dried on a hot plate at 40 – 50 °C under a stream of N_2. The recovery of the SPE procedure was 63 ± 7% (n = 12).

2.2.2 Riverbed sediment organic matter

Riverbed sediments of the Kolyma main stem were sampled using a Van Veen grab-sampler, sampling surface sediment up to 1 – 5 cm, and stored in sterile Whirl-Pak® bags. These samples represent recently deposited sediment (i.e., with a large fraction of silt and clay) in more quietly flowing locations of the river and delta. Within 12 hours after collection, sediments were frozen (-20 °C) and remained so during transport. At the laboratory at the Vrije Universiteit Amsterdam, the samples were freeze-dried, and sieved through a 200 µm and a 63 µm mesh, resulting in three size fractions of sediment: coarse sand (>200 µm), fine sand (63-200 µm) and a combination of silt and clay (<63 µm).

Particles coarser than silt (>63 µm) are quickly deposited during sediment transport, and carry little mineral-associated OC, while the fine sediment fraction (<63 µm) carries the bulk of the mineral-associated OC (Coppola et al., 2007; Keil et al., 1994; Tesi et al., 2016), and is considered to represent an integrated signal of suspended matter transported by the river (Freymond et al., 2018). Therefore, in this study, we focus only on the fine, easily transportable fraction of the sediment. The term "SOC" ~~in this paper~~here therefore refers to the OC content of the < 63 µm sediment fraction. This fractionation step allows us to cross-compare the same fraction of sediment and OC at different locations along the river transect and beyond, on the shelf, despite the heterogeneity of bulk sediments.

2.3 Mineral-specific surface area analysis

For mineral surface area (SA) measurements, subsamples of about 1.5 g freeze-dried sediment were combusted at 450 °C for 12 h to remove OC, rinsed twice with MilliQ to remove salt and ashes, and freeze dried again. Directly prior to analysis, the samples were degassed for a minimum of 2 hours at 300 °C under vacuum. The analyses were performed at the Vrije Universiteit Amsterdam on a Quantachrome Nova 4200e, using the 6-point Brunauer–Emmett–Teller method (Brunauer et al., 1938). The SA measurements were regularly checked against two certified reference materials (5.41 $m^2 g^{-1}$ and 27.46 $m^2 g^{-1}$).

2.4 Bulk elemental analyses

2.4.1 Carbon concentrations and stable carbon isotope analyses

Concentration of DOC and DOC-$\delta^{13}C$ were analysed with an Aurora1030 TOC analyser coupled to a Delta V Advantage isotope ratio mass spectrometer (IRMS) at KU Leuven (Belgium), ~~see further~~following the method ~~details in~~of ~~-~~Deirmendjian et al. (2020).

The POC concentrations, and POC-$\delta^{13}C$ were measured on a combined elemental analyser - isotope ratio mass spectrometer (EA-IRMS) at the National Research Council Institute of Polar Sciences (Bologna, Italy). Before subsampling, the concentration of ~~suspended particulate matter (~~SPM~~)~~ was determined by weighing the sediment loaded filters after freeze-drying and dividing by the volume of water filtered. A s~~S~~ubsample~~s were~~ was punched out of each ~~the~~ 47 mm GF/F filter~~s~~, placed in a pre-combusted silver capsule~~s~~, and weighed. Inorganic C was removed by adding 50 µl of 1 M HCl twice to the silver capsules. After oven drying (over NaOH pellets to neutralise acid, at 60 °C), the silver capsules were wrapped in tin capsules to aid combustion during analysis.

Sediment (<63 µm fraction) was crushed and homogenized in an agate mortar, and two subsamples of each sample were weighed into pre-combusted silver capsules for total OC and $\delta^{13}C$ analyses. The sediment was acidified ~~in~~ as described above for the filters to remove inorganic C, wrapped in tin capsules after acidification and measured for OC at the Sediment Laboratory and for $\delta^{13}C$ at the Stable Isotope Laboratory of the Vrije Universiteit Amsterdam (The Netherlands). All $\delta^{13}C$ values are reported in ‰ relative to the international standard VPDB (Vienna Pee Dee Belemnite).

2.4.2 Radiocarbon analyses

Radiocarbon (^{14}C) analyses were carried out using an EA coupled to a MICADAS accelerator mass spectrometer (AMS) at the Laboratory of Ion Beam Physics of the Swiss Federal Institute of Technology (ETH, Zürich, Switzerland), following the method described in McIntyre et al. (2017). A second subsample of the GF/F filters (POC) was punched-out ~~Subsampled filters (POC)~~ and a subsample of sediment (SOC) was taken and~~were~~ weighed in pre-combusted silver capsules for ^{14}C analyses~~, and~~. For these samples. inorganic carbon was removed by fumigation in a desiccator with 37% HCl at 60 °C for 72 h (Komada et al., 2008). After fumigation, samples were dried over NaOH pellets at 60 °C for 72 h to neutralize the acid, and wrapped in tin capsules. The final ^{14}C results are corrected for constant background contamination using the method described in Haghipour et al. (2018). All radiocarbon data are presented either as $\Delta^{14}C$ (‰) or as conventional, uncalibrated radiocarbon age (yr) (Stuiver and Polach, 1977).

2.5 Molecular and biomarker analyses

2.5.1 CuO oxidation products

Microwave-assisted alkaline CuO oxidation was carried out at the laboratory of the Vrije Universiteit Amsterdam to extract lignin and cutin products from SPE-DOC and SOC samples, following the method of Goñi & Montgomery (2000). In summary, Teflon extraction vessels were loaded with ~2 – 4 mg OC, 500 mg CuO and 50 mg ferrous ammonium sulfate. For SPE-DOC samples, 10 mg of glucose was added to prevent superoxidation of lignin polymers. Then, 10 mL of degassed 2 N NaOH solution was added under oxygen-free conditions. The oxidation was performed using a MARS 6 microwave (CEM Cooperation) at 150 °C (1,600 W, 8 min ramp, continued heating for 90 min). The resulting extract was centrifuged, transferred to a pre-combusted glass vial, and an internal recovery standard (Ethyl vanillin; Sigma-Aldrich) was added. The samples were acidified to pH 1 by adding concentrated HCl, and then extracted twice with ethyl acetate. The samples were dehydrated with anhydrous ~~sodium sulfate~~Na_2SO_4, transferred to combusted amber glass vials, and dried under flow of N_2. Prior to analyses on an Agilent gas chromatograph-mass spectrometer (GC-MS) at the National Research Council Institute of Polar Sciences (Bologna, Italy), samples were re-dissolved in pyridine and methylated with BSTFA. The individual lignin phenols, benzoic acids, and *p*-hydroxybenzenes were quantified by comparison with commercially available standards, and quantification of cutin-derived products was done using the response of trans-cinnamic acid.

2.5.2 Lipid biomarker analyses

For the extraction of lipid biomarkers from POC, ~~one to three~~ freeze-dried 90 mm GF/F filters~~, each containing 3 to 26 mg of POC,~~ were selected ~~per location~~ and placed in pre-extracted Teflon extraction vessels. For some locations, multiple filters (up to three~~3~~) had to be extracted to obtain enough material (~6 to 26 mg OC). For riverbed SOC, ~2 g of sediment was weighed in per extraction vessel, containing ~12 – 17 mg ~~of~~ OC. Samples were solvent-extracted twice with 15 ml DCM:MeOH (9:1 v/v) at 100 °C (1,600 W, 5 min ramp, continued heating for 15 min), using a MARS 6 microwave (CEM Cooperation). The resulting extract was saponified with 10 – 15 ml of KOH in methanol (0.5 M) at 70 °C for 2 h. Subsequently, 5 – 10 ml of MilliQ water with 2% NaCl was added. The neutral fraction (containing *n*-alkanes) was extracted with hexane (3 x 10 ml), after which the samples were acidified to pH 2 with concentrated HCl. The acid fraction was then extracted with hexane:DCM (4:1 v/v), methylated with BF_3-MeOH (80 °C, 30 min), and extracted with DCM after addition of MilliQ water. The acid fraction was further cleaned of impurities by column chromatography (SiO_2, water-deactivated), by eluting first with hexane, then DCM:hexane (4:1) and DCM. The cleaned methylated *n*-alkanoic acids, concentrated in the DCM:hexane fraction, were then analysed on a GC-MS at the National Research Council Institute of Polar Sciences (Bologna, Italy). Quantification of high molecular weight (HMW; carbon chain length 24 – 30) *n*-alkanoic acids was done by comparison with commercially

available standards (alkanoic acid C22, C24, C26, C28 and C30; Sigma-Aldrich). The carbon preference index (CPI) of the HMW *n*-alkanoic acids is calculated as the ratio between even and odd carbon chain lengths (Eq. 1).

$$CPI = \frac{\left(\frac{1}{2}*[C23+C25+C27+C2\ ]\right)+\left(\frac{1}{2}*[C25+C27+C29+C\ \ ]\right)}{[C24+C26+C28+C30]}, \quad (1)$$

2.6 Endmember analyses

Source apportionment models are commonly used to distinguish different source contributions to the total OC pool based on their isotopic signature. Dual-carbon isotope endmember mixing models have proven to be useful tools to disentangle the various sources of organic matter in different environments, as these Markov chain Monte Carlo (MCMC) techniques account for uncertainties in both the endmember values as well as the uncertainties in sample measurements and thus provide better constraints on the relative contributions of different sources to bulk OC (Andersson et al., 2015; Bosch et al., 2015; Vonk et al., 2012; Wild et al., 2019). For this sample set, we identified three different OC sources that contributed to the POC and SOC, and calculated their relative fractions using a dual-isotope $\delta^{13}C$ and $\Delta^{14}C$ endmember mixing model. Our approach combines an isotopic mass-balance source apportionment model, Bayesian MCMC, which uses dual-isotope signatures (endmembers) from bulk OC to differentiate between the following three sources: i. Permafrost OC; ii. Modern vegetation and surface soil OC; iii. Riverine primary production OC (for the Kolyma samples) or Marine primary production OC (for the ESS samples). We defined the endmember for permafrost OC as a mixture of Pleistocene Ice complex deposits (ICD) and Holocene permafrost (including Holocene peat), with a~~n~~ $\delta^{13}C$ value of -26.3 ± 0.7‰ (Vonk et al., 2012) and a $\Delta^{14}C$ value of -761.2 ± 120‰. Thise $\Delta^{14}C$ value was derived as the mean of the ICD endmember (-954 ± 65.8‰; n = 329; Wild et al., 2019) and the Holocene/peat permafrost endmember (-567 ± 157‰; n = 138; Wild et al., 2019) assuming approximately equal carbon stock input of these two pools in this region (Zimov et al., 2006a). Different weighing of these two permafrost OC pools (e.g., spatial area-weighing of ICD coverage giving a $\Delta^{14}C$ value of -683.7 ± 136‰) did not significantly change the result of the model. The endmember for the second source, modern vegetation and surface soil OC (including the active layer, soil OC and recent vegetation; hereafter "vegetation/soil OC"), was adapted from Wild et al. (2019) with a $\delta^{13}C$ value of -27.2 ± 1.1‰ (n = 150) and a $\Delta^{14}C$ value of -52.7 ± 137.3‰ (n = 118). Wild et al. (2019) presented endmembers of these sources separately, but due to the inclusion of a primary production source as a third source, we ~~we prefer to~~ combined them as one contemporary terrestrial endmember.~~,~~ ~~t~~Therefore, their values were averaged, equally weighted to one endmember. The third source, primary production OC (fluvial or marine), has an endmember $\delta^{13}C$ value of -32.1 ± 3.0‰ and a $\Delta^{14}C$ value of +11.0 ± 37 for riverine samples (henceforth named "Riverine PP OC"), while the endmember for marine samples ("Marine PP OC") is $\delta^{13}C$ = -24.0 ± 3‰, $\Delta^{14}C$ = +60 ± 60‰ (Vonk et al., 2012). The riverine PP OC endmember is based on a compilation of samples and using the endmember values of previous studies: $\delta^{13}C$ = -30.5 ± 2.5 ‰, $\Delta^{14}C$ = +41.9 ± 4.2 ‰ (Winterfeld et al., 2015a), $\delta^{13}C$ = -30.6 ± 3.3‰, $\Delta^{14}C$ = +48 ± 11‰ (Wild et al., 2019), and the sample of ~~our own algal bloom sample from~~ the Panteleikha River from this study ($\delta^{13}C$ = -33.5‰, $\Delta^{14}C$ = -26‰), where an algal bloom was observed during the study period. For the marine $\delta^{13}C$ endmember (-24.0 ± 3‰), we also tested a value of -21 ± 1‰, used in Bröder et al. (2016) for ESS sediments. The modelling results showed a minimal, non-significant change for SOC in endmember contributions (Fig. A2~~1~~). However, for POC, there was a large shift on the first part of the marine transect from POC being marine PP dominated to being vegetation/soil OC dominated using the -21 ± 1‰ endmember (Fig. A2~~1~~). This is probably related to the sharp transition from a riverine PP to a marine PP endmember, while in reality the transition is not as sharp and likely a mixture of these two sources within the estuary. The contribution of the permafrost endmember to the POC pool was not significantly affected by this shift. Increasing or decreasing the standard deviation of either of the marine PP endmembers (-24 and -21‰) from ± 1 ‰ to ± 3‰ did not make a difference.

The dual-isotope/three-sources version of the MCMC source apportionment model was adapted from Bosch et al. (2015). We used MATLAB (version 2021a) to model contributions of the three different sources, with the following model parameters:

1,000,000 iterations, a burn-in (initial search phase) of 10,000, and a data thinning of 10. For further details on the method see (Andersson et al., 2015; Andersson, 2011; Bosch et al., 2015).

3 Results and Discussion

The Kolyma River transports fluvial organic matter towards the East Siberian Sea in three different compartments; the dissolved, particulate and sedimentary OC pools. Our study targets all these compartments and adds a spatial dimension by not only sampling along a 250-km main stem transect, but also including a range of tributaries, and extending the riverine transect ~1000 km across the ESS using existing data (SI Table 1; Bröder et al., 2019; Salvadó et al., 2016; Tesi et al., 2014; Vonk et al., 2010a). In contrast to previous studies (e.g., Bröder et al., 2020; McClelland et al., 2016), we do not focus on the seasonal OC variability within fluvial systems (i.e., comparing different stages of the hydrograph), but aim to convey a consolidated picture of riverine dissolved, particulate and sedimentary OC delivered to the East Siberian Sea, and to give insight on the processes that affect these OC pools along the land-ocean continuum.

3.1 Three contrasting OC pools: Concentrations of DOC, POC and SOC

In Arctic rivers, DOC and POC concentrations vary significantly during seasons ~~(Bröder et al., 2020; Holmes et al., 2012; McClelland et al., 2016)~~. Concentrations found in this study (Table 2) match the typical range of DOC and POC values of the Kolyma River in the late summer season ~~(Table 2)~~(Bröder et al., 2020; Holmes et al., 2012; McClelland et al., 2016). The DOC concentrations along the Kolyma River transect range from 2.76 to 4.97 mg L^{-1}, which ~~are on the same order of magnitude as~~is a bit higher than DOC in ESS surface waters (~0.6 – 1.8 mg L^{-1}; Salvado et al., 2016; Alling et al., 2010). The POC concentrations during this period, range from 1.49 to 2.73 mg L^{-1}, and show a rapid decrease once offshore in the ESS, from 2.7 mg L^{-1} at location K6 to 0.2 mg L^{-1} approximately 50 km farther at location YS34B (at water depth 10 m; Vonk et al., 2010a, Fig. 1). The Kolyma tributaries PAN and Y3 show notably higher DOC and POC concentrations of 21.5 and 9.71 mg L^{-1} DOC, and 4.50 and 2.38 mg L^{-1} POC, respectively, compared to the Kolyma. The sample DY TS shows extremely high concentrations of DOC (103 mg L^{-1}) and POC (> 7,300 mg L^{-1}), which are in the same range as other thaw streams at this location (Vonk et al., 2013). Sample DY KOL, located right at the outflow of a thaw stream into the Kolyma River, shows that the extremely high concentrations of DOC and POC coming from DY thaw streams are quickly diluted by river water and/or settles rapidly to the riverbed. The DOC concentration in this sample is in the same range as the Kolyma main stem (2.75 mg L^{-1}), while the POC concentration remains elevated at 103 mg L^{-1}. The SOC concentrations in the <63 µm fraction of riverine sediment show values ranging from 0.45 to 1.0% (~~average~~ 0.76 ± 0.19%, mean ± standard deviation, n = 5) along the Kolyma River transect, which are slightly lower than ESS SOC (which was not sieved) with concentrations between 0.80 and 1.76% (~~average~~ mean of 1.15 ± 2.94%, n=18; Salvadó et al., 2016; Vonk et al., 2010a). The fraction of OC in particulate matter (OC concentrations normalized to TSS) is much higher than in SOC, ranging from 6.7 to 12.8% within the Kolyma and with values up to 47% for the Pantaleikha, pointing towards a significant contribution of primary production (i.e., pure organic matter without minerals) to the particulate load.

Table 2. Bulk data for sediment organic carbon (SOC), dissolved organic carbon (DOC) and particulate organic carbon (POC). Including concentrations, surface area (SA), organic carbon loading and isotopic data $\delta^{13}C$, $\Delta^{14}C$, conventional, uncalibrated radiocarbon age (yr), and fraction modern (Fm) with the measurement error.

Short ID	SOC	SA	OC loading	Grain size		$\delta^{13}C$	$\Delta^{14}C$	^{14}C age	Fm	Fm error
Sediment <63 µm	wt.%	$m^2\ g^{-1}$	mg OC m^{-2}	median µm		‰	‰	yr.		±
Kolyma										
K 2	0.82	9.6	0.85	39.5		-27.1	-521	5850	0.483	0.003
K 3	0.66	8.7	0.75	39.4		-26.9	-586	7020	0.418	0.004
K 4	1.00	11.9	0.84	37.0		-27.1	-530	6000	0.474	0.003
K 5	0.88	11.9	0.74	31.5		-27.4	-537	6120	0.467	0.005
K 6	0.45	8.4	0.54	46.8		-27.2	-579	6890	0.424	0.004
Duvanny Yar										
DY PF	0.63	13.4	0.47	34.5		-26.1	-965	26800	0.036	0.001
DOC and POC	**DOC**	**DOC $\delta^{13}C$**	**POC**	**POC**	**SPM**	**POC $\delta^{13}C$**	**POC $\Delta^{14}C$**	**POC ^{14}C age**	**Fm**	**Fm error**
	mg L^{-1}	‰	mg L^{-1}	wt.%	mg L^{-1}	‰	‰	yr.		±
Kolyma										
K 1	2.76	-28.3	1.42	12.8	11.2	-31.6	-221	1940	0.785	0.010
K 2	2.96	-30.0	1.71	6.68	25.6	-29.0	-379	3760	0.627	0.007
K 3	3.60	-30.0	1.71	7.28	23.5	-29.8	-306	2870	0.700	0.008
K 4	3.49	-29.4	1.49	8.12	18.4	-30.0	-362	3540	0.643	0.007
K 5	3.23	-28.8	1.67	9.10	18.4	-30.7	-296	2750	0.710	0.010
K 6	4.97	-27.3	2.73	8.12	33.7	-29.9	-301	2810	0.705	0.008
Duvanny Yar										
DY TS	103	-29.8	7325	1.22	~~600363~~ 6.00 × 10^5	-25.5	-860	15730	0.141	0.002
DY KOL	2.75	-28.7	15.7	4.50	348	-26.3	-859	15670	0.142	0.003
Tributaries										
BA	4.43	-29.5	1.70	7.85	21.7	-31.3	-175	1480	0.832	0.009
MA	3.16	-28.9	1.29	15.9	8.11	-33.3	-348	3370	0.658	0.006
Y3	21.5	-29.4	2.38	18.3	13.0~~2~~	-32.5	-160	1500	0.830	0.010
PAN	9.71	-31.2	4.50	46.6	9.67	-33.5	-26	145	0.984	0.010

3.2 Three contrasting OC pools: Isotopes of DOC, POC and SOC

Each organic carbon pool (DOC, POC and SOC) shows distinctly different stable carbon isotope ($\delta^{13}C$) and radiocarbon isotope ($\Delta^{14}C$) ratios, which are important tools in characterising OC and tracing OC from different sources. The DOC-$\delta^{13}C$ along the Kolyma River transect ranges from -27.3 to -30.0‰ (Table 2), which is comparable to earlier published data (Feng et al., 2013; Mann et al., 2015; Wild et al., 2019). Although we have not measured DOC-$\Delta^{14}C$ in this work, earlier studies show that Kolyma River and tributary DOC is relatively young ($\Delta^{14}C$ in the range of +150 to -100‰; Neff et al., 2006; Wild et al., 2019). The DOC-$\delta^{13}C$ of the tributaries and Duvanny Yar are in the same range as the Kolyma, except for sample PAN, which shows a ~~more depleted~~lower $\delta^{13}C$ value of -31.2‰. An earlier study on a Duvanny Yar thaw stream found DOC-$\Delta^{14}C$ values between -974 and -911 ‰ (up to 30,000 yr old) (Vonk et al., 2013). However, such old ~~aged~~ DOC has not been found in the main Kolyma River, likely due to rapid turnover times of permafrost DOC in Arctic waters (Rogers et al., 2021).

The $\delta^{13}C$ of Kolyma POC ranges from -29.0 to -31.6‰, and the $\Delta^{14}C$ ranges from -221 to -379‰, corresponding to 1,940 to 3,760 yr (Fig. 2). The $\delta^{13}C$ values of the Kolyma transect correlate with POC% (the OC weight % of dried particulate matter; $R^2 = 0.91$, $p < 0.01$) and $\Delta^{14}C$ ($R^2 = 0.79$, $p < 0.01$), in other words, samples with a high POC% have a more depleted $\delta^{13}C$ value and a ~~less depleted~~less negative (younger) $\Delta^{14}C$ value, both supporting a significant contribution from riverine production. The tributary and Duvanny Yar samples are clearly different from the Kolyma in their isotopic signature of POC: the two Duvanny Yar POC samples are ~~more enriched~~higher in $\delta^{13}C$ (-25.5 and -26.3‰), and have a substantially ~~more~~ lower $\Delta^{14}C$ ~~depleted~~ (-859 and -860‰; 15,700 yr) than Kolyma POC, while the other tributaries (PAN, MA, BA and Y3) show generally ~~more depleted~~lower $\delta^{13}C$ values (-31.3 to -33.5‰) and ~~younger~~ higher (i.e. younger) $\Delta^{14}C$ values (-26 to -348‰; 145 to 3,370 yr) than Kolyma POC. The $\Delta^{14}C$-POC values in the Kolyma (K1-K6) are in the same range as Kolyma summer POC of 2013 and 2015 (-314 ± 83‰, n = 38; Bröder et al., 2020; Fig. 2), and slightly younger than the ~~average~~ mean Kolyma summer POC between 2003 and 2011 (-463 ± 15‰, n = 32; McClelland et al., 2016).

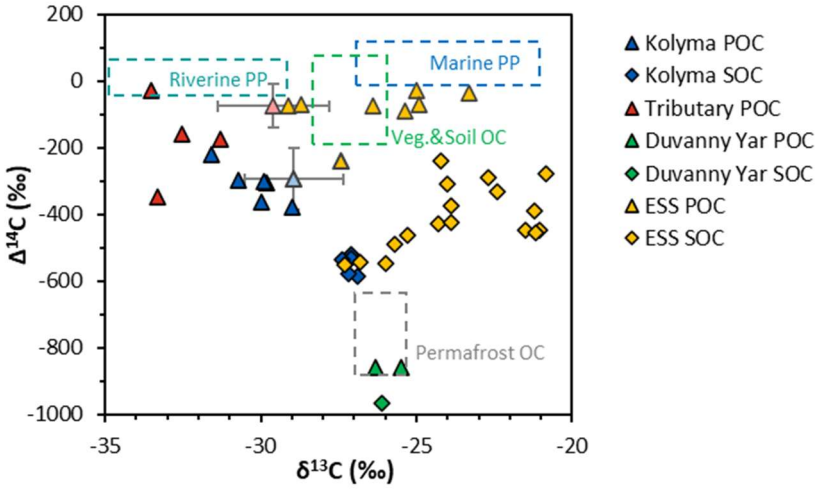

Figure 2. $\Delta^{14}C$ versus $\delta^{13}C$ values of the Duvanny Yar (DY), Kolyma, tributary, and East Siberian Sea (ESS) samples. Triangles are POC samples, diamonds are SOC samples. Kolyma main stem in dark blue, ESS in yellow, tributaries in red and DY in green. The boxes represent the endmembers as defined in section 2.6. The triangles with standard deviation show the ~~average~~ mean ± standard deviation of Kolyma particulate organic carbon (POC, faded blue) and Y3, one of the tributaries, POC (faded red) samples of Bröder et al. (2020) for reference.

These trends in $\delta^{13}C$ and $\Delta^{14}C$ in POC point towards the influence of a younger, more ^{13}C-depleted source of OC in the Kolyma River and especially in the tributaries. A similar trend was found in Bröder et al. (2020), suggesting influence of riverine primary production. In situ production of OC by fluvial organisms in Arctic rivers and streams has not received a lot of attention, but frequently displays very low ~~depleted~~ $\delta^{13}C$ ~~signatures~~ values (e.g., -30.5 ± 2.5‰ in Winterfeld et al. (2015a) Lena River; -30.6 ± 3.3‰ Ob and Yenisey rivers, Galimov et al. (2006); -33.4 ± 4.2‰ in Shakil et al. (2020), streams on the Peel Plateau). The lower $\delta^{13}C$ values of heterotrophic OC are due to contributions of recycled CO_2 that sources from terrestrial organic matter breakdown, which is already relatively ~~depleted~~ low in $\delta^{13}C$ (Meyers, 1994). Winterfeld et al. (2015a) applied a source-apportionment approach to Lena River POC in summer and found that primary production accounted for up to 80% of the fluvial POC. This 'recycled carbon' (Wild et al., 2019) appears to be an important component of summer POC transport, which is reflected in the overall ~~δ~~^{13}C-depleted values in the Kolyma River and tributaries POC pool (Fig. 2, and section 3.3). Comparing the carbon isotope data of fluvial POC collected in this study with surface water POC collected along the extended Kolyma River transect in the ESS shows a large difference between the terrestrial and marine samples (Fig. 2; Fig. 3b and d). The ESS POC is distinctly younger than Kolyma POC: $\Delta^{14}C$ values between -28 and -75‰ for the inner ESS and between -69 and -240‰ for the outer ESS, and similarly ~~more enriched in~~ less negative $\delta^{13}C$: ranging from -23.3 to -29.1‰, with a trend towards ~~more enriched~~higher values moving from the river mouth farther offshore (Salvadó et al., 2016; Vonk et al., 2010a).

We find that Kolyma SOC is distinctly older ($\Delta^{14}C$ of -521 to -586‰; 5,850 to 7,020 yr) and ~~less depleted~~shows less negative ~~in~~ $\delta^{13}C$ than POC, displaying a narrow range in $\delta^{13}C$ values (-26.9 to -27.4‰) (Fig. 2; Fig 3a, c). On the other hand, Kolyma River SOC is distinctly younger than the Yedoma permafrost material from Duvanny Yar (Fig. 2). The Yedoma permafrost sample DY PF shows an extremely ~~depleted~~ low $\Delta^{14}C$ value of -965‰ (26,800 yr), and a slightly ~~less depleted~~higher $\delta^{13}C$ ~~value~~ratio than Kolyma POC ~~of -26.1‰~~. The ESS SOC close to shore shows a similar age as the Kolyma SOC in this study, with a trend towards ~~less depleted~~less negative $\Delta^{14}C$ values farther offshore (-624 to -332‰, $\Delta^{14}C$). In ESS SOC-$\delta^{13}C$, a trend can be seen moving from -27.1 ‰, close to ~~the value of~~ Kolyma SOC, towards ~~more enriched~~higher $\delta^{13}C$ values of -22.4‰ farther offshore (Fig. 3a). This increase in $\delta^{13}C$ and $\Delta^{14}C$ values of POC and SOC moving from river to shelf is likely due to the increased contribution of marine PP OC to the SOC and POC pools farther offshore, together with sorting and settling of terrestrial and permafrost-derived OC (Bröder et al., 2018; Tesi et al., 2014; Vonk et al., 2012), processes that will be discussed in more detail in the next sections.

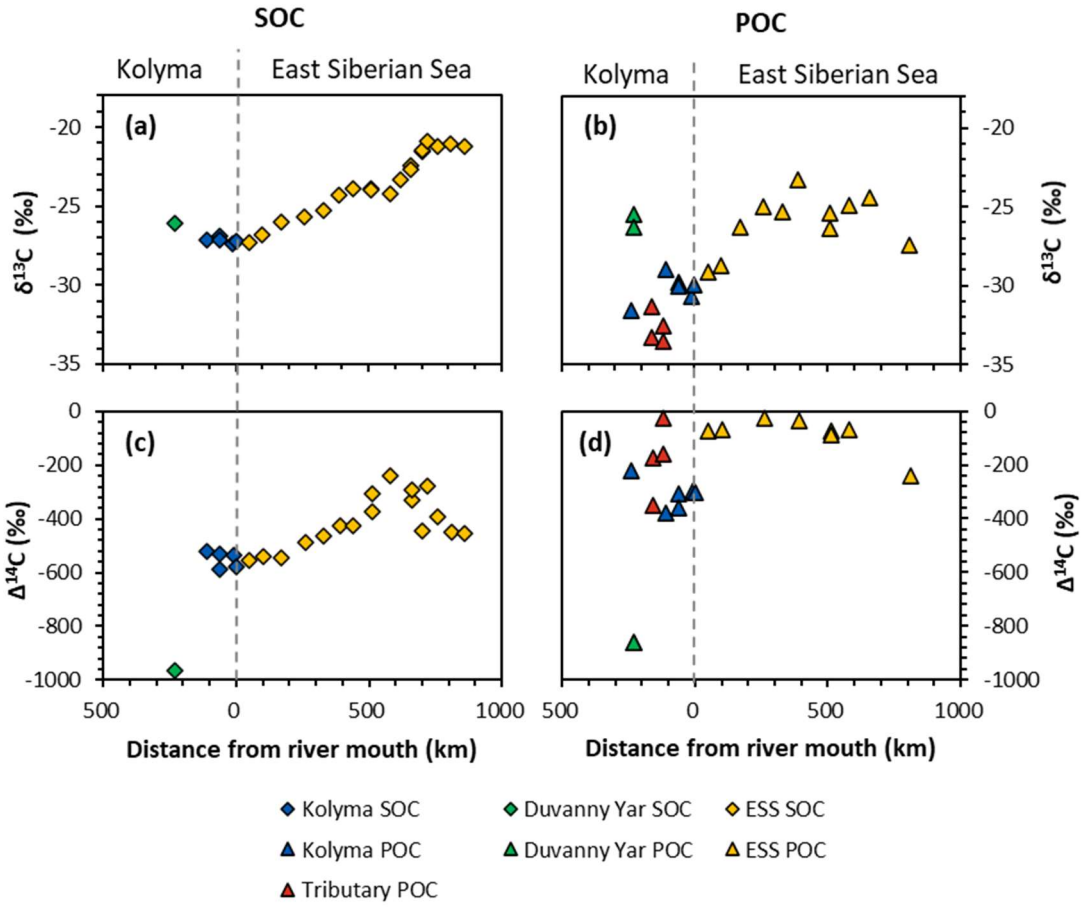

Figure 3. Carbon isotopes over transect distance, with the riverine part on the left side of each figure, and the marine part on the right. (a) $\delta^{13}C$ ratio (in ‰ relative to VPDB) of Duvanny Yar (DY; green), Kolyma (blue) and East Siberian Sea (ESS; yellow) sediment organic carbon (SOC). (b) $\delta^{13}C$ ratio of DY (green), Kolyma (blue), tributaries (red), and ESS (yellow) particulate organic carbon (POC). (c) $\Delta^{14}C$ ratio of DY, Kolyma and ESS SOC. L~~The l~~ower ~~the~~ $\Delta^{14}C$ ratios~~, the~~ indicate older ~~the material~~OC ~~is~~. (d) $\Delta^{14}C$ ratio of DY, Kolyma, tributaries and ESS POC.

3.3 Quantifying the sources of OC: End member mixing analyses

The $\Delta^{14}C$ and $\delta^{13}C$ signatures of POC and SOC can be used to quantify the relative contributions of different organic carbon sources (i.e., permafrost OC; vegetation/soil OC; riverine PP OC for the Kolyma and marine PP OC for the ESS) to these two carbon pools, following the method described in section 2.6. We revisit the endmember mixing results from Vonk et al., (2012) for the ESS and from Wild et al., (2019) for the Kolyma River to connect river and shelf environments with the newly defined endmembers (see section 2.6 for endmember definitions). Relative contributions of the different sources varied considerably between POC and SOC, and Kolyma and ESS (Fig. 4).

Along the river transect, Kolyma River main stem POC consists largely of riverine PP OC (44 ± 10%), while the tributary POC shows even higher ~~values~~ riverine PP OC contributions of 64 ± 10% ~~on average~~(mean ± standard deviation). ~~Particularly the Pantaleikha POC stands out with a 79 ± 11% riverine PP OC contribution, which agrees with our field observation of an algal bloom at the time of sampling.~~ The contribution of vegetation/soil OC is roughly equal for POC and SOC, ranging from ~~on average~~ 18 ± 14% in Kolyma main stem POC, 15 ± 11% in tributary POC and 19 ± 12% in Kolyma SOC. Permafrost OC is the dominant source in Kolyma SOC (~~on average~~ 68 ± 10%), and the second largest contributor to the Kolyma main stem POC (38 ± 8%). As expected, the contribution of permafrost OC is highest in Duvanny Yar POC and SOC samples (93 ± 4%). Source apportionment modelling on the Kolyma POC data from Bröder et al. (2020) shows that the ~~average~~ mean contribution of permafrost OC to Kolyma POC is in the same range (38 ± 9%) as in this study over their whole sampling period (ranging from s~~S~~pring 2012 to f~~F~~all ~~of 2012 to~~ 2015), while the ~~average~~ contribution of vegetation/soil OC is slightly (26 ± 16%) higher, and the ~~average~~ contribution of riverine PP OC is slightly (37 ± 12%) lower than in the samples of this study. This could be due to the timing of the sampling; Bröder et al. (2020) also include the early and late summer when riverine PP may not be high, while our study likely includes the peak of the riverine PP production. At tributary Y3, including this dataset, the ~~average~~ contribution of permafrost OC is only 11 ± 6%. The bulk of the POC in Y3 comes from the other two sources: 51 ± 19% from riverine and 38 ± 20% from vegetation/soil, which is in line with the conclusion of Bröder et al. (2020), that the Y3 tributary does not have the ~~power~~ erosional force to ~~erode~~ mobilize ~~deeper into the~~ permafrost.

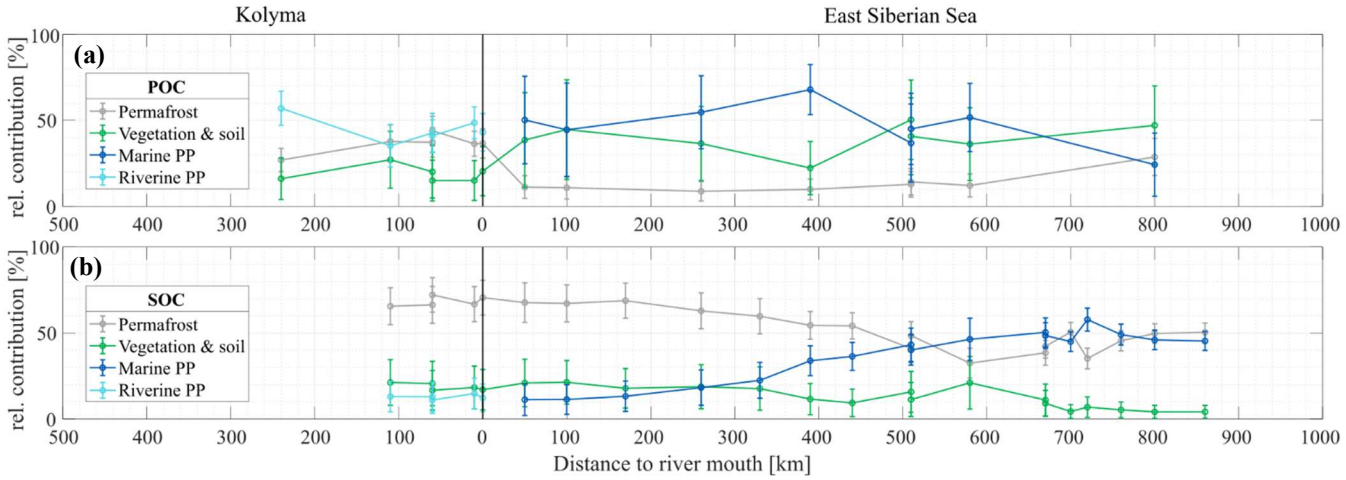

Figure 4. Mean relative contribution (± standard deviation from Monte Carlo simulations) of three endmembers over transect distance for (a) ~~Relative contribution of three endmembers over transect distance for~~ **(a) surface water particulate organic carbon (POC) and (b) sediment organic carbon (SOC), based on dual carbon isotope ($\Delta^{14}C$ and $\delta^{13}C$) endmember analyses ~~(EMMA)~~. For the riverine part of the transect (Kolyma; left side of the figure), the endmembers are: Permafrost organic carbon (OC) in grey, Vegetation/soil OC in green, and Riverine primary production (PP) OC in cyan. For the marine part of the transect (East Siberian Sea; right side of the figure), the endmembers are: Permafrost OC in grey, Vegetation/soil OC in green, and Marine primary production OC in dark blue. Definition of the endmembers are described in section 2.6 and can be seen Fig. 2.**

For the marine transect, the riverine primary production endmember was 'replaced' with the marine primary production endmember, since marine primary production is absent in the river, and riverine primary production OC is thought to be rapidly recycled in a marine setting, which is supported by the rapid shift towards a ~~less depleted~~higher $\delta^{13}C$ ~~signature~~ ratio of POC in the first part of the offshore ESS transect. Marine primary production appears to be the dominant source of POC in the ESS, supplying roughly half of the OC along the entire ESS transect (~~average~~ 47 ± 12%). Furthermore, we find similar results as Vonk et al., (2012; 2010) for ESS SOC: an increase in the contribution of marine PP OC (from 10% to ~50%; Fig. 4b), and a steady decrease of the two terrestrial endmembers farther offshore. Notably, the permafrost OC endmember remains the dominant source of OC up to 500 km offshore, decreasing from 70% to ~40%, before marine PP OC becomes dominant. Note that we have not incorporated lateral transport times of sediment OC (estimated up to 3600 yr. across the Laptev shelf; Bröder et al., 2018) that affect all terrestrial OC during sedimentary transport. In contrast, for POC we find an initial sharp decrease in the contribution of permafrost OC, from ~40% in the Kolyma River to ~10% at the first transect point offshore (Fig. 4a),

remaining around 10% for the entire length of the transect. Likely, the permafrost OC consists mostly of mineral-bound OC, material that has been shown to rapidly settle in the near-shore region (Jong et al., 2020; Karlsson et al., 2011; Vonk et al., 2010b), which may explain the high permafrost contribution to the SOC pool and rapid decrease of permafrost OC in the POC pool. On the contrary, primary production biomass and organic debris is not mineral-bound and can ~~remain afloat~~be transported over long distances (Karlsson et al., 2011; Vonk et al., 2010b; Tesi et al., 2016), which is reflected in the relatively high contributions of these pools in the POC of the ESS.

3.4 Sources of OC: lignin biomarker concentrations and proxies

Terrigenous biomarkers such as lignin derived phenols, cutin-derived hydroxy fatty acids and HMW *n*-alkanoic acids can be used to further trace the source, pathway, and fate of OC in rivers and in the marine environment (e.g., Freymond et al., 2018; Tesi et al., 2014). The lignin content, either normalised to OC content (as mg g^{-1} OC^{-1}) or to mineral surface area (as µg m^{-2}), refers to the sum of vanillyl (V), syringyl (S) and cinnamyl (C) phenols, and is an indicator for the contribution of higher vascular plant material to the total organic matter pool (Goñi & Hedges, 1992). The ratios between lignin phenol groups S/V and C/V can be used for tracing the various types of plants generating these phenols (Hedges and Mann, 1979). These lignin source proxies have been extensively used to characterize and trace different pools of OC on land, in rivers and in the marine environment (e.g., Amon et al., 2012; Goñi et al., 2000).

The lignin concentrations in DOC of the Kolyma transect range from 1.70 to 5.11 mg g^{-1} OC^{-1} (Table 3), and the DOC lignin concentration in the four tributaries (MA, PAN, Y3 and BA) are in the same range as the Kolyma transect (3.61 to 5.62 mg g^{-1} OC^{-1}). These are in the same range as earlier results in the Kolyma River (4.7 mg g^{-1} OC; Feng et al., 2017; 6.5 mg g^{-1} OC Amon et al., 2012). Sample DY TS is a notable exception, with a higher lignin concentration of 11.79 mg g^{-1} OC^{-1}. For the ESS, only a few dissolved lignin concentrations are published, and they are an order of magnitude lower than in the Kolyma River, at roughly 0.2 mg g^{-1} OC^{-1} at four points in the outer ESS (Salvadó et al., 2016). Lignin concentrations in Kolyma SOC (<63 um) range from 6.46 to 14.87 mg g^{-1} OC^{-1}, which is clearly higher than in DOC, but lower than in the first two sampling points in the ESS (not sieved; 28.40 and 16.00 mg g^{-1} OC^{-1}; Salvadó et al., 2016). Farther offshore, the lignin concentrations in SOC gradually decrease to 0.10 mg g^{-1} OC^{-1}, indicating a decreasing influence of terrestrial biomass on the total OC pool, which is supported by the bulk C isotopes (Salvadó et al., 2016).

A similar pattern is evident in cutin concentrations. For the Kolyma transect, they range from 0.40 to 1.35 mg g^{-1} OC^{-1} for DOC and 2.18 to 5.67 mg g^{-1} OC^{-1} for SOC. The cutin concentrations of the four tributaries are in the same range (0.52 to 1.23 mg g^{-1} OC^{-1}) as for Kolyma DOC, while in the Duvanny Yar thaw stream (DY TS) the concentrations are much higher at 4.79 mg g^{-1} OC^{-1}. The cutin to lignin ratio is higher for SOC than for DOC in the main Kolyma samples (0.40 ± 0.12 versus 0.21 ± 0.11, respectively; Fig. A3~~2~~), which could be due to a methodological bias: the SOC cutin to lignin ratio could be artificially raised by the sieving step while processing the sediments, thus the lignin-rich organic debris could remain in the coarse fraction (Tesi et al., 2016).

To further pinpoint the source of higher plant-derived OC, ratios between lignin phenol groups (C/V and S/V) can be used to distinguish different vegetation sources: woody versus non-woody material and gymnosperm versus angiosperm material (Hedges & Mann, 1979; Goñi & Hedges, 1992; Goñi & Montgomery, 2000). The S/V and C/V ratios show fairly consistent values for the Kolyma transect DOC, with an S/V ratio of 0.41 to 0.48 and a C/V ratio of 0.12 to 0.18 (Fig. 5). For the Kolyma SOC, the S/V and C/V ratios are slightly higher than those for DOC (0.51 to 0.54 and 0.21 to 0.48). These ratios indicate a roughly equal mix of gymnosperm and angiosperm material in both DOC and SOC within the Kolyma main stem (Fig. 5), and an equal mix of woody and non-woody material in DOC. This is in accordance with earlier studies on the sources of DOC in the Kolyma River (Amon et al., 2012), and indicative of the mixed vegetation of the Kolyma watershed (taiga- and tundra vegetation). The DOC sample DY TS appears to consist~~s~~ completely of non-woody angiosperm organic matter, with very high S/V and C/V ratios of 0.97 and 0.31, respectively. However, the DOC sample at DY KOL and the permafrost SOC sample

DY PF show to be more of a mix of angiosperm and gymnosperm soft tissue material (S/V 0.55, C/V 0.33), in the same range as Kolyma SOC and DOC, and in line with other studies on Yedoma deposits (Winterfeld et al., 2015b; with 0.51 – 1.24 for S/V and 0.27 – 1.07 for C/V, Lena Delta Pleistocene and Holocene deposits).

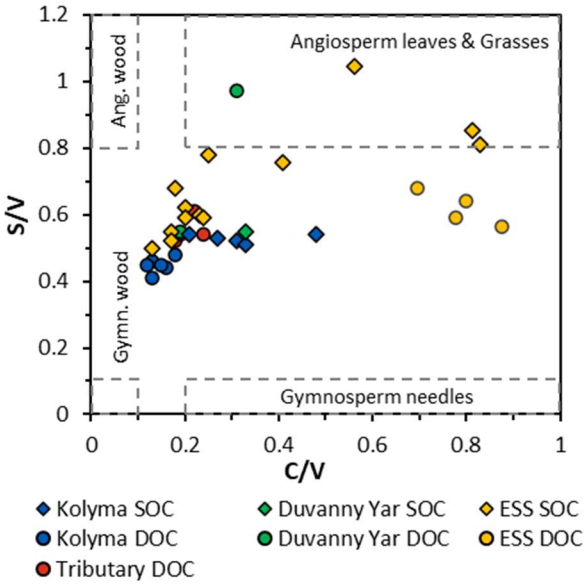

Figure 5. The ratios between syringyl/vanillyl (S/V) and cinnamyl/vanillyl (C/V) can be used as biomarker source proxies for sediment organic carbon (SOC; diamonds), dissolved organic carbon (DOC; circles) ~~and particulate organic carbon (POC; triangles)~~ from the Kolyma River (blue), Duvanny Yar (green), East Siberian Sea (ESS; yellow) and a ~~couple~~few smaller tributaries of the Kolyma (red). Ranges for v~~V~~egetation and tissue types ~~(~~boxes~~)~~ are based on (Goñi et al., 2000).

3.5 Sorting and degradation of OC along the land-ocean continuum: OC and biomarker loading

Changes in surface area normalized concentrations (i.e., loadings) of terrestrial OC at bulk and molecular level, measured across coastal shelves (e.g., Tesi et al., 2016; Bröder et al., 2018) and along riverine transects (e.g., Freymond et al., 2018), provide means to quantify loss of OC due to degradation (Aller & Blair, 2006; Keil et al., 1997). Due to the large variability in hydrodynamic conditions and heterogeneous sediments found within a river, and even more so along a river to shelf transect, it is necessary to trace a specific fraction (e.g. through a consistent method of sediment fractionation) to be able to directly compare sediments across dynamic land-ocean transects. Mineral SA normalization is useful for the fraction high in mineral-bound OC (generally the <63 µm fraction: silt and finer), but works less well on sediment with either large fractions of non-mineral bound carbon (e.g., loose organic debris) or material low in mineral-bound OC (e.g., coarse sand). In addition, the <63 µm fraction is the most easily transported fraction of sediment in rivers, even at lower flow velocities, and is thus the fraction that is transported farthest offshore, as coarse organic debris and sand quickly settles near the coasts (Tesi et al., 2016; Wakeham et al., 2009).

The SA-normalised OC-loadings of the <63 µm river sediment range from 0.54 to 0.85 mg OC m^{-2}, with no apparent trend along the main stem transect. These OC loadings are within the range of "typical" river-influenced sediments (0.4 – 1.0 mg OC m^{-2}; (Keil et al., 1994; Mayer, 1994; Blair & Aller, 2012), and similar to OC loadings found in other river systems (Freymond et al. (2018); Danube River; similar sediment sampling protocol). The loading of OC on Kolyma sediment is ~~and are~~ on average higher than for the surface sediments of the ESS (Bröder et al., 2019; 0.19 to 0.46 mg OC m^{-2}), and ~~that also show~~ a decreasing trend in OC loadings can be seen with increasing distance from land/water depth (Fig. 6a), suggesting that loss of mineral-bound OC occurs during offshore transport (Keil et al., 1997).

For biomarkers, the SA-normalized lignin concentrations of Kolyma River sediment vary between 5.13 and 12.67 µg m^{-2} (Fig. 6~~a~~b), while the SA-normalized cutin concentrations are lower, ranging between 1.17 and 4.18 µg m^{-2} (Fig. 6~~d~~b). The SA-normalised HMW acid concentrations are between 2.26 and 2.92 µg m^{-2} (Fig. 6~~c~~e). For Duvanny Yar, the OC and biomarker loadings are lower than for Kolyma sediments, due to the combination of high SA and lower OC and biomarker concentration. Freymond et al. (2018) found HMW *n*-alkanoic acid loadings of 0.4-1.5 µg m^{-2}, and lignin loadings between 0.6 and 26.4 µg

500 m^{-2} in sediments from the Danube River and its tributaries, using the same sampling and similar extraction methods, which is on the same order of magnitude as for the Kolyma River.

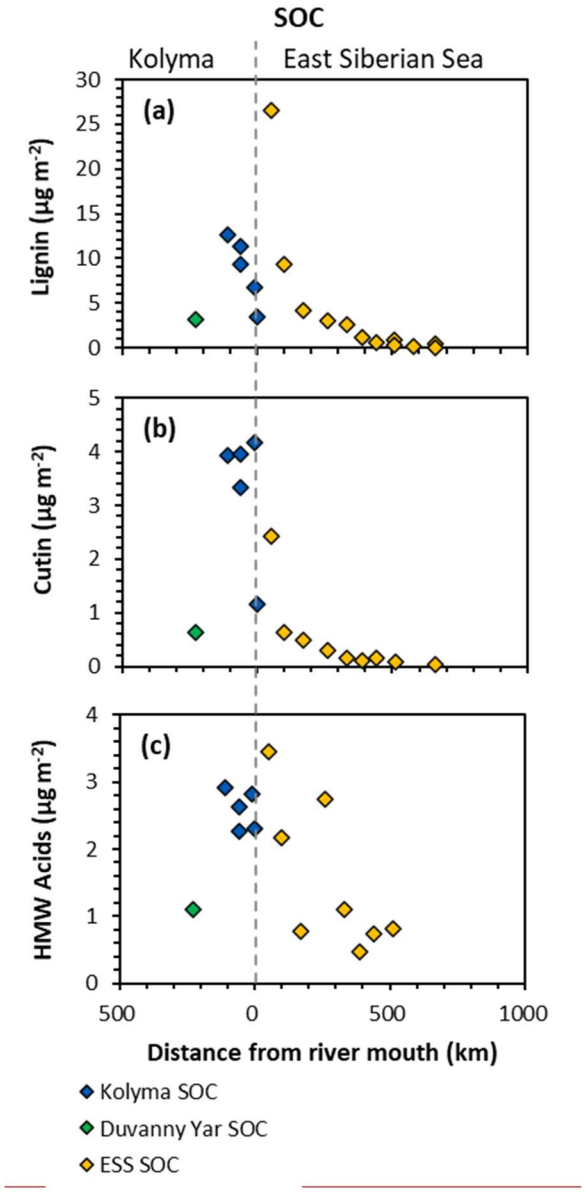
SOC
Kolyma
East Siberian Sea
(a)
Lignin (μg m-2)
(b)
Cutin (μg m-2)
(c)
HMW Acids (μg m-2)
Distance from river mouth (km)
Kolyma SOC
Duvanny Yar SOC
ESS SOC

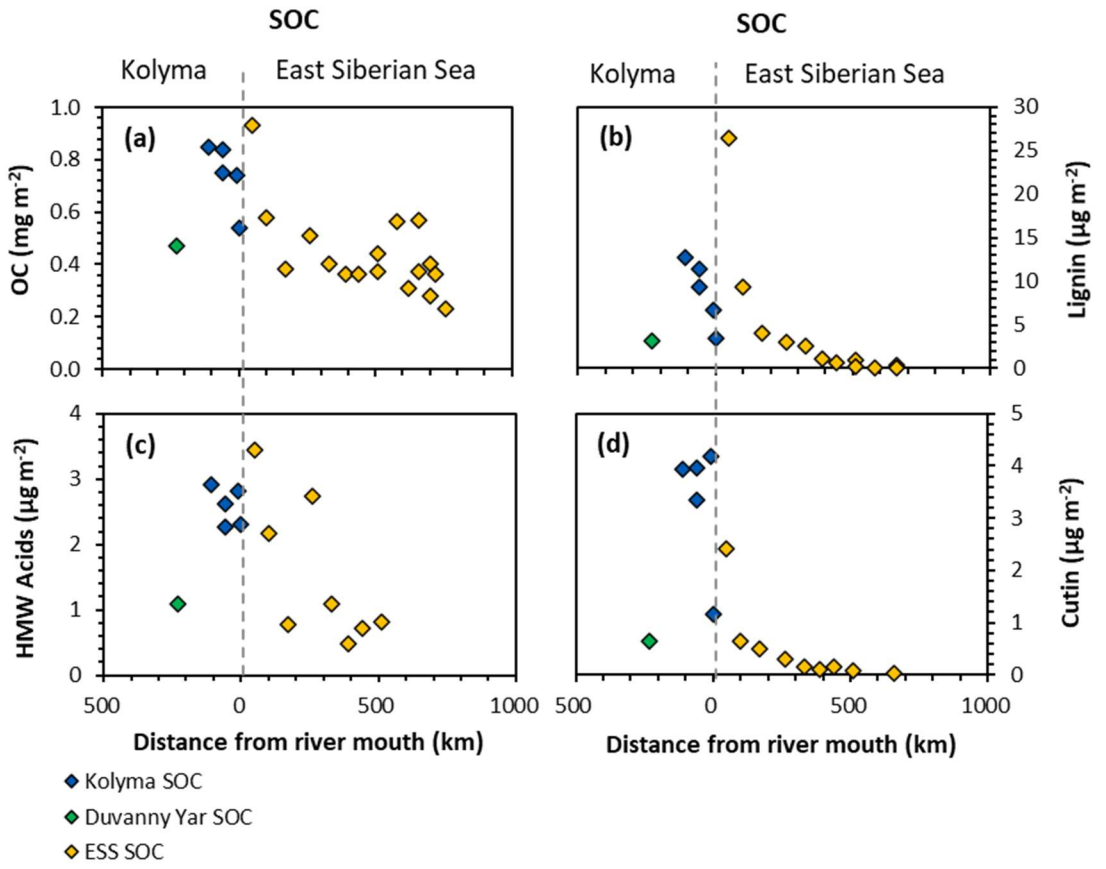

Figure 6. Organic carbon and bBiomarker concentrations normalised to mineral surface area over transect distance for the Kolyma (blue), Duvanny Yar (green), and East Siberian Sea (ESS; yellow) sediment organic carbon (SOC) samples. (a) OC concentrations (mg m^{-2}), (ba) Lignin concentrations (µg m^{-2}), (cb) Cutin concentrations (µg m^{-2}), and (ed) HMW *n*-alkanioc acids (C24 – C30) concentrations (µg m^{-2}).

Along the ESS transect sediments, a sharply decreasing trend in lignin loadings was found in earlier studies (Karlsson et al., 2011; Tesi et al., 2014; Vonk et al., 2010a), from 28.4 µg m^{-2} near the coast down to 0.1 µg m^{-2} on the outer shelf (Fig. 6ba), and a similar trend for cutin, from 2.4 to 0.1 µg m^{-2} (Fig. 6d5b), and HMW acids from 3.4 to 0.8 µg m^{-2} (Fig. 6ce) ~~(Karlsson et al., 2011; Tesi et al., 2014; Vonk et al., 2010a)~~. When comparing the marine end of the riverine transect with the shallowest sample of the marine transect, the lignin and cutin concentrations seem disconnected at this riverine-marine interphfasce: the lignin loadings of the riverine sediment samples appear lower than expected while the cutin concentrations appear higher than expected, which is also reflected in the cutin/lignin ratios (Fig. A32). Only the riverine HMW *n*-alkanoic acid concentrations align well with the beginning of the marine transect. This discrepancy in behaviour of different biomarkers could be due to their different affinity towards mineral particles. We recognise that we are comparing sieved (<63 µm) riverbed samples with non-sieved (bulk) marine samples but as Tesi et al., (2016) showed that 88 – 95% of the marine sediments in the eastern part of the ESS consist of the <63 µm fraction, we do not ~~think that~~expect this size difference ~~it~~to be~~s~~ the main contributor to the observed discrepancy. Instead, earlier sediment partitioning studies that fractionated sediments by both density and size, found that lignin is mostly present in the low-density fraction (<1.8 g mL^{-1}) as coarse organic debris (Wakeham et al., 2009; Tesi et al., 2016). It is true that low-density material is often relatively large in size, which in our case (sieving river sediments through 63 µm) places low density material in the coarse fraction. This may explain the lower concentrations of lignin for the riverine transect. In contrast, cutin-derived acids are more closely associated to fine mineral particles, and HWM *n*-alkanoic acids are more evenly distributed among sediment fractions (Tesi et al., 2016), explaining the better match of these two biomarker groups in comparing Kolyma <63 µm sediment to the ESS transect.

Freymond et al. (2018) propose normalizing OC and biomarkers to SA as the benchmark for comparing river and marine sediments. However, our results point out that this approach seems to work only for certain biomarker groups, since the method

we apply based on Freymond et al. (2018), appears to underestimate lignin and overestimate cutin concentrations. Therefore, we propose to use sediment fractionation methods not purely on size but also on density, and to apply these techniques consistently for all samples, ideally along transects that stretch across the entire river to– shelf continuum. While multiple fractionation steps are often time and labour intensive, our results suggest that fractionating only by size (i.e., sieving over 63 µm) is not enough to completely resolve sorting and degradation dynamics of terrestrial OC across the dynamic land-ocean interface, since certain biomarker groups have affinity for different (density) fractions of the sediment.

3.6 Degradation state of OC along the land-ocean continuum: biomarker proxies

The relative abundances of specific lignin phenol compound classes can be used as proxies for the overall degradation status of organic carbon, for instance, the acid/aldehyde ratios of vanillyl (Vd/Vl) and syringyl (Sd/Sl) phenols are often used as an indicator for degradation of plant organic matter (Hedges et al., 1988; Opsahl & Benner, 1995). More degraded lignin yields more acids relative to aldehydes in the CuO extraction process, which is reflected in ~~The aldehydes degrade faster than the corresponding acids, meaning that~~ a higher Vd/Vl ~~or~~and Sd/Sl ratio ~~indicates more degraded material~~. However, these ratios are also influenced by leaching and adsorption processes (Hernes et al., 2007). Another CuO-oxidation product that is frequently used as a degradation indicator is 3,5-dihydroxybenzoic acid (3,5Bd), due to the recalcitrant nature of 3,5Bd, the ratio 3,5Bd/V increases with OC degradation in soils and sediments (Houel et al., 2006). In addition to CuO-oxidation products, the ratio between odd and even HMW *n*-alkanoic acids, the carbon preference index (CPI), can be used as a degradation proxy. The CPI is indicative of organic matter maturity, since fresh plant material has a strong even-over-odd preference for *n*-alkanoic acids (Freeman and Pancost, 2014; Eglinton and Hamilton, 1967), which is lost with ongoing degradation. Thus, organic matter with lower CPI values is considered to be more degraded.

SOC and DOC in the Kolyma River display distinctly different Vd/Vl and Sd/Sl ratios. The SOC shows low values of Vd/Vl and Sd/Sl, ranging from 0.21 to 0.48 and 0.39 to 0.47, respectively (Fig. 7a, c), indicating that SOC is relatively fresh and not degraded. In contrast, the DOC shows higher values, indicating more degradation~~-~~, with Vd/Vl ranging from 1.77 to 2.35, and Sd/Sl ranging from 1.06 to 1.39 (Fig. 7b, d). Similarly, the 3.5Bd/V ratios are lower for Kolyma SOC (0.07 – 0.14) than for DOC (0.20 to 0.32) (Fig. 7e. f). In the tributaries, a wider range of Sd/Sl and Vd/Vl ratios was found in DOC, ranging from 0.67 to 3.83 and from 1.22 to 4.89, respectively. Notably, the Yedoma thaw stream (DY TS) shows the highest Vd/Vl and Sd/Sl ratio, and, in contrast, the lowest 3,5Bd/V ratio among all DOC samples, meaning it is fresh in terms of 3,5Bd/V, but

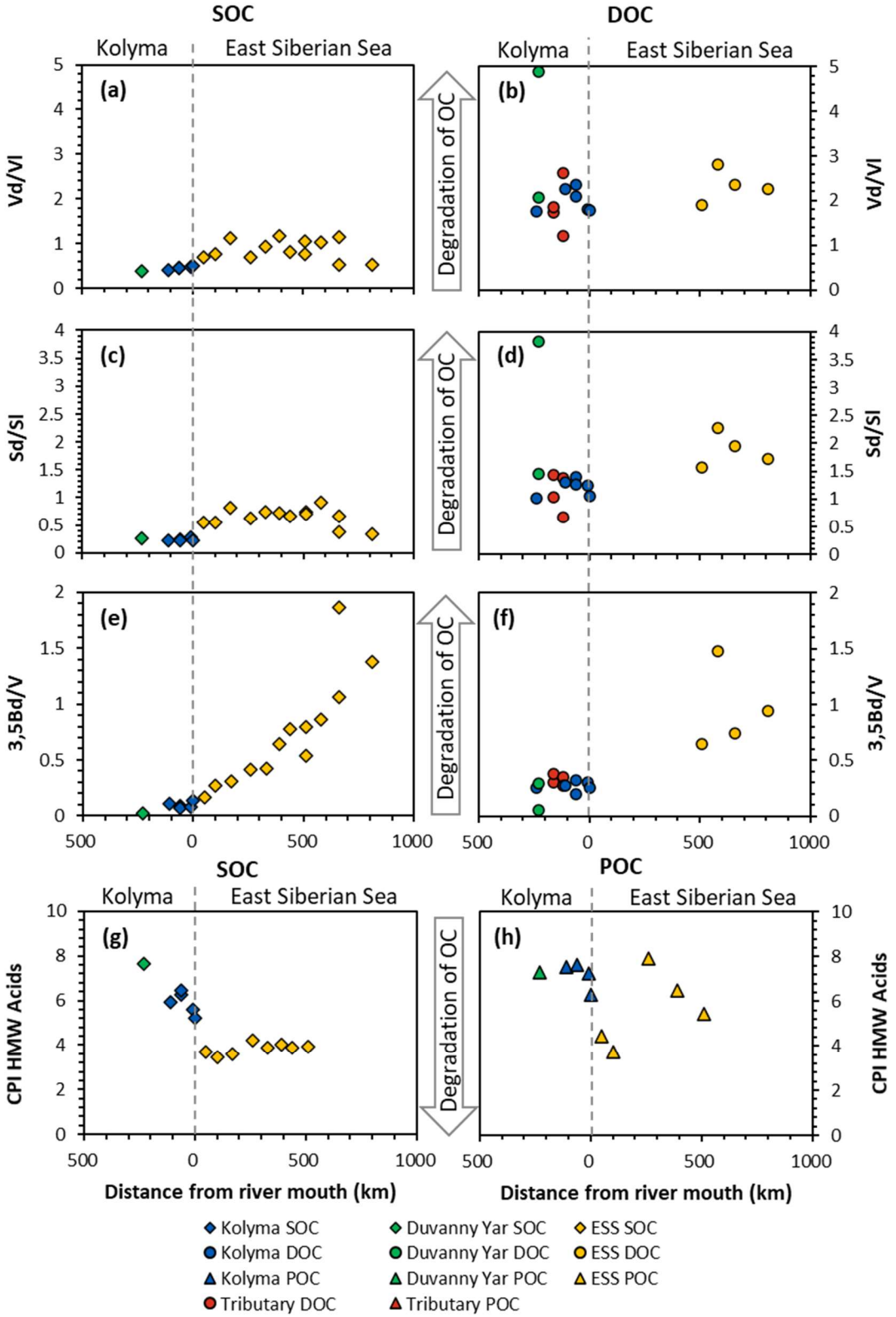

Figure 7. Biomarker degradation proxies of sediment organic carbon (SOC; diamonds), dissolved organic carbon (DOC; circles) and particulate organic carbon (POC; triangles) from the Kolyma River (blue), Duvanny Yar (green), East Siberian Sea (ESS; yellow) and a couple smaller tributaries of the Kolyma (red) over transect distance. For visual aid the arrows in the middle point towards more degraded values. (a) Acid/aldehyde ratio of Vanillyl phenols (Vd/Vl) of SOC, and (b) of DOC. (c) Acid to aldehyde ratio of Syringyl phenols (Sd/Sl) of SOC, and (d) of DOC. (e) 3,5Bd/V ratio of SOC, and (f) DOC. (g) the carbon preference index of HMW *n*-alkanoic acids (C24 – C30) of SOC, and (h) of POC.

Table 3. Molecular biomarker data for sediment organic carbon (SOC), dissolved organic carbon (DOC), and particulate organic carbon (POC).

Short ID	Lignin Λ		Cutin		Cutin/Lignin	S/V	C/V	Sd/Sl	Vd/Vl	3,5-Bd/V	HMW acids*		CPI
Sediment <63 µm	mg g^{-1} OC^{-1}	µg m^{-2}	mg g^{-1} OC^{-1}	µg m^{-2}							µg g^{-1} OC^{-1}	µg m^{-2}	
Kolyma													
K 2	14.87	12.67	4.62	3.94	0.31	0.53	0.27	0.23	0.41	0.11	3430	2.92	5.94
K 3	12.46	9.39	5.26	3.96	0.42	0.52	0.31	0.25	0.45	0.09	3002	2.26	6.27
K 4	13.43	11.34	3.95	3.34	0.29	0.51	0.33	0.22	0.45	0.07	3114	2.63	6.45
K 5	9.19	6.77	5.67	4.18	0.62	0.54	0.48	0.29	0.47	0.08	3836	2.83	5.60
K 6	6.46	3.46	2.18	1.17	0.34	0.54	0.21	0.22	0.49	0.14	4309	2.31	5.20
Duvanny Yar													
DY PF	6.75	3.15	1.36	0.64	0.20	0.55	0.33	0.27	0.39	0.02	2344	1.09	7.65
DOC											**POC**		
Kolyma													
K 1	3.11		1.35		0.43	0.44	0.16	1.02	1.77	0.25	27^		
K 2	4.24		0.96		0.23	0.41	0.13	1.31	2.27	0.27	798		7.56
K 3	4.24		0.66		0.16	0.46	0.13	1.39	2.35	0.32	271		7.63
K 4	5.11		0.59		0.12	0.45	0.15	1.27	2.1	0.2	99^		
K 5	1.7		0.40		0.24	0.45	0.12	1.24	1.8	0.3	254		7.25
K 6	5.08		0.44		0.09	0.48	0.18	1.06	1.78	0.25	368		6.32
Duvanny Yar													
DY TS	11.79		4.79		0.41	0.97	0.31	3.83	4.89	0.05			
DY KOL	5.31		1.27		0.24	0.55	0.19	1.45	2.06	0.29	898		7.3
Tributaries													
BA	5.62		0.52		0.09	0.52	0.18	1.03	1.74	0.3			
MA	3.61		1.23		0.34	0.61	0.22	1.43	1.85	0.38			
Y3	4.6		0.54		0.12	0.54	0.19	0.67	1.22	0.35			
PAN	4.99		0.61		0.12	0.54	0.24	1.37	2.61	0.27			

* HMW *n*-alkanoic acids with chain lengths C24 – C30

^ Not enough to calculate CPI

degraded ~~in terms of~~according to Vd/Vl and Sd/Sl. The CPI of HMW *n*-alkanoic acids, measured in SOC and POC, is slightly lower (i.e., more degraded) in SOC (5.20 to 6.45) than in POC (6.32 to 7.63) in the Kolyma River, while sample DY PF shows a higher (i.e., fresher) CPI of 7.65 (Fig. 7g, h). In an earlier study on Yedoma permafrost (or "ice complex deposits") in the Lena Delta (Sánchez-García et al., 2014), a wide range of CPI values was found, between 3.0 and 12.0. The CPI of HMW *n*-alkanoic acids of Sánchez-García et al. (2014) (mean of 6.6 ± 2.7, n = 17) is however very close to our sample DY PF. For two POC samples (K1 and K4), odd HMW *n*-alkanoic acid concentrations were below the detection limit, so the CPI of these two samples could not be calculated.

When connecting the Kolyma transect to the ESS, both the Vd/Vl, Sd/Sl and 3,5Bd/V ratios are consistently higher in ESS sediments than in Kolyma sediments (Fig. 7a, c, e). While Vd/Vl and Sd/Sl show no clear trend across the entire transect, the trend in 3,5Bd/V appears to connect well with the riverine transect, with increasing ratios (i.e., more degraded OC) farther offshore. For DOC, data from the outer ESS show similar Vd/Vl ratios, and slightly higher Sd/Sl and 3,5Bd/V ratios than riverine DOC (Fig. 7b, d, f). The CPI of ESS SOC clusters around ~4 (Fig. 7g), which is considerably lower (i.e., more degraded) than Kolyma SOC. For POC, the CPI does not show a clear trend across the river-shelf transect (Fig. 7h), however, it remains higher (i.e., fresher) than SOC, which is in line with the results of Salvadó et al., (2016).

Our results for all four degradation proxies (Vd/Vl, Sd/Sl, 3.5Bd/V, and HMW *n*-alkanoic acid CPI ~~acids~~) in the sedimentary OC pool suggest that riverine SOC is less degraded than its marine counterpart, likely due to the relatively short residence time of SOC in rivers (years to decades; Repasch et al., 2021; Hilton et al., 2015), as compared to SOC in shelf sediments (centuries to millenia; Bröder et al., 2018). Additionally, we found that~~The overall pattern found in this study is a rapid change in almost all parameters moving from freshwater to the marine environment.~~ w~~W~~ithin the river there is relatively little change with~~not much change over~~ distance downstream, and, similarly, the changes over distance on the marine side are limited~~slow~~ or very gradual. However, ~~, but o~~in the relatively short (ca. 30-50 km) ~~within~~transition zone between the freshwater system and the marine system there is a large change~~big shift~~ in most measured dissolved, particulate and sedimentary parameters ~~for DOC, POC and SOC~~.

When one looks at patterns across different pools such as DOC versus SOC or POC versus DOC, the patterns are more ambiguous. This is likely caused by (i) a variety of processes such as leaching, sorption or fractionation that are at play between these pools, in addition to (ii) the temporal aspect that is different for DOC and POC (daily to seasonal snapshots) than SOC (integrating several years to decades). Generally, however, we can say that SOC and POC appear relatively fresh (despite having a high radiocarbon age) and DOC appears more degraded (yet with a lower radiocarbon age), as is also found in previous studies (Feng et al., 2017; Goñi et al., 2000; Salvadó et al., 2016; Tesi et al., 2014; Vonk et al., 2013, 2010). The SOC pool is the main (temporary) storage place for permafrost thaw-derived OC, and we propose to devote more scientific attention to the physical and chemical processes affecting the transport and degradation of this fraction, as eventually this will determine the fraction of permafrost OC that can be captured for long term-burial.

4 Conclusions and outlook

The aim of this study was to use an integrated approach to investigate the changes of different phases of OC (dissolved, particulate and sediment OC), and the effect of fractionation and degradation on permafrost-derived OC during transport over large distances along the land-ocean continuum. We conclude that permafrost-derived OC makes up the bulk of the total SOC along the source-to-sink system, and accounts for a significant part of the POC in the Kolyma River. In contrast, the contribution of permafrost-derived OC is marginal to POC in the marine realm and to DOC across the entire transect, despite the presence of ^{14}C depleted sources within the watershed. Overall, this highlights the importance of accounting for all carbon pools in order to allow for comparisons between fluvial and marine systems across different temporal scales.

We found a decrease in OC and terrigenous biomarkers normalised to sediment mineral surface area across the transect, indicating loss through degradation of terrestrial OC over transport distance, and especially pronounced changesshifts in the transition zoneon the border between the freshwater and marine realm. Molecular biomarker proxies indicating OC degradation show a remarkably "fresh" biomarker signature for SOC, despite its generally lower $\Delta^{14}C$ values (i.e. older) than DOC and POC. Biomarker degradation proxies along the land-ocean continuum generally compare well between river samples and marine samples, yet show diverse degradation patterns when comparing between different OC pools (e.g., DOC versus SOC). Processes such as leaching and sorption, causing transfer of OC between DOC and POC pools, may explain some of the patterns we observed, in addition to the contrasting timescales that these pools represent (from days to years). We therefore want to emphasize that an integrated approach is necessary to obtain a complete picture of OC transport along the river-ocean continuum, and recommend to (a) minimally compare one pool (e.g., SOC) across land-ocean transects, and ideally (b) compare all pools (SOC, POC, DOC) consistently across land-ocean transects. Furthermore, as we here have shown that permafrost-derived OC is mostly transported within the SOC fraction, we recommend to increaseincreasing scientific focus on the sedimentary fraction when studying the fluvial and marine fate of permafrost OC.

Finally, we want to acknowledge that large discrepancies remain between the freshwater and marine research fields when studying OC dynamics as marine studies seem to focus mostly on SOC, while river studies mostly target DOC. It is necessary to connectLinking these two environments and make sure to (i) applying common consistent methodology, and (ii) increase emphasis on the dynamic terrestrial-marine transition zone is necessary in order toto completely resolve the fate of terrestrial OC along river-shelf systems, with a focus on the dynamic transition zone between the terrestrial and the marine realm.

Appendix

Table A1. East Siberian Sea (ESS) sample locations, names, and distance from the mouth of the Kolyma River for sediment samples, surface water dissolved organic carbon samples (DOC) and surface water particulate organic carbon samples (POC). Data used in this study was gathered from four earlier publications: Bröder et al., 2019; Salvadó et al., 2016; Tesi et al., 2014; Vonk et al., 2010. Specifically, Tesi et al., (2014) and Vonk et al. (2010) have characterized surface water DOC and POC in the ESS, along with underlying surface sediments, following the paleo river valley of the Kolyma up to 600 km offshore, collected on 3-5 September 2008, and data from a more recent cruise (between 31 July and 4 August 2014) are used to extend this transect up to 1000 km offshore (Bröder et al., 2019; Salvadó et al., 2016).

Sample name/site	Latitude (°)	Longitude (°)	Distance from river mouth (km)	Water depth (m)	References for data
Sediment					
YS034B	69.71	162.69	-50	10	Tesi et al., 2014; Vonk et al., 2010
YS035	69.82	164.06	-100	31	Tesi et al., 2014; Vonk et al., 2010
YS036	69.82	166.00	-170	32	Tesi et al., 2014; Vonk et al., 2010
YS037	70.13	168.01	-260	42	Tesi et al., 2014; Vonk et al., 2010
YS038	70.70	169.13	-330	36	Tesi et al., 2014; Vonk et al., 2010
YS039	71.22	169.37	-390	44	Tesi et al., 2014; Vonk et al., 2010
YS040	71.48	170.55	-440	49	Tesi et al., 2014; Vonk et al., 2010
YS041	71.97	171.79	-510	43	Tesi et al., 2014; Vonk et al., 2010
YS086	75.30	174.40	-760	200	Tesi et al., 2014; Vonk et al., 2010
YS088	75.10	172.19	-700	142	Tesi et al., 2014; Vonk et al., 2010
YS090	74.67	172.39	-660	63	Tesi et al., 2014; Vonk et al., 2010
YS091	74.43	170.85	-620	56	Tesi et al., 2014; Vonk et al., 2010
SWE-60	73.52	169.46	-510	43	Bröder et al., 2019; Salvadó et al., 2016
SWE-61	74.11	170.90	-580	51	Bröder et al., 2019; Salvadó et al., 2016
SWE-63	74.68	172.37	-660	64	Bröder et al., 2019; Salvadó et al., 2016
SWE-64	74.94	172.69	-700	120	Bröder et al., 2019
SWE-65	75.16	173.19	-720	170	Bröder et al., 2019
SWE-66	75.90	174.30	-810	239	Bröder et al., 2019; Salvadó et al., 2016
SWE-67	76.32	175.61	-860	468	Bröder et al., 2019; Salvadó et al., 2016
DOC					
SWE-60	73.52	169.46	-510		Salvadó et al., 2016
SWE-61	74.11	170.90	-580		Salvadó et al., 2016
SWE-63	74.68	172.37	-660		Salvadó et al., 2016
SWE-66	75.90	174.30	-810		Salvadó et al., 2016

Table A1. (cont.)

Sample name/site	Latitude (°)	Longitude (°)	Distance from river mouth (km)	References for data
POC				
YS-34B	69.71	162.69	-50	Tesi et al., 2014; Vonk et al., 2010
YS-35	69.82	164.06	-100	Tesi et al., 2014; Vonk et al., 2010
YS-36	69.82	166.00	-170	Tesi et al., 2014; Vonk et al., 2010
YS-37	70.13	168.01	-260	Tesi et al., 2014; Vonk et al., 2010
YS-38	70.70	169.13	-330	Tesi et al., 2014; Vonk et al., 2010
YS-39	71.22	169.37	-390	Tesi et al., 2014; Vonk et al., 2010
YS-40	71.48	170.55	-440	Tesi et al., 2014; Vonk et al., 2010
YS-41	71.97	171.79	-510	Tesi et al., 2014; Vonk et al., 2010
SWE-60	73.52	169.46	-510	Salvadó et al., 2016
SWE-61	74.11	170.90	-580	Salvadó et al., 2016
SWE-63	74.68	172.37	-660	Salvadó et al., 2016
SWE-66	75.90	174.30	-810	Salvado et al., 2016

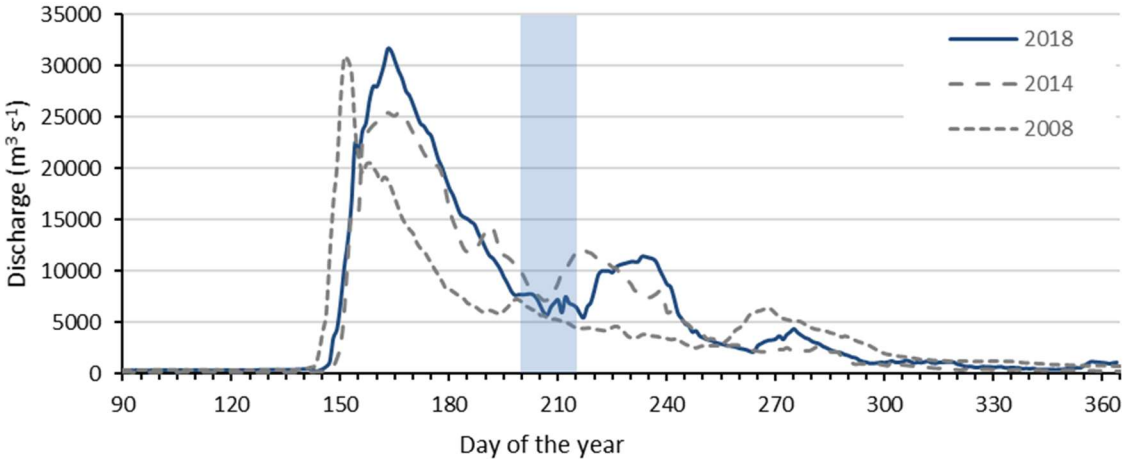

Figure A1. Discharge of the Kolyma River at Kolymskoye, about 40 km upriver of sampling point K 1, in 2018 (Shiklomanov et al., 2021, Artic GRO dataset). Sampling period of this study highlighted in blue, directly after spring freshet. In grey dotted lines the discharge of the Kolyma River during the 2008 and 2014 East Siberian Sea sampling campaigns for comparison.

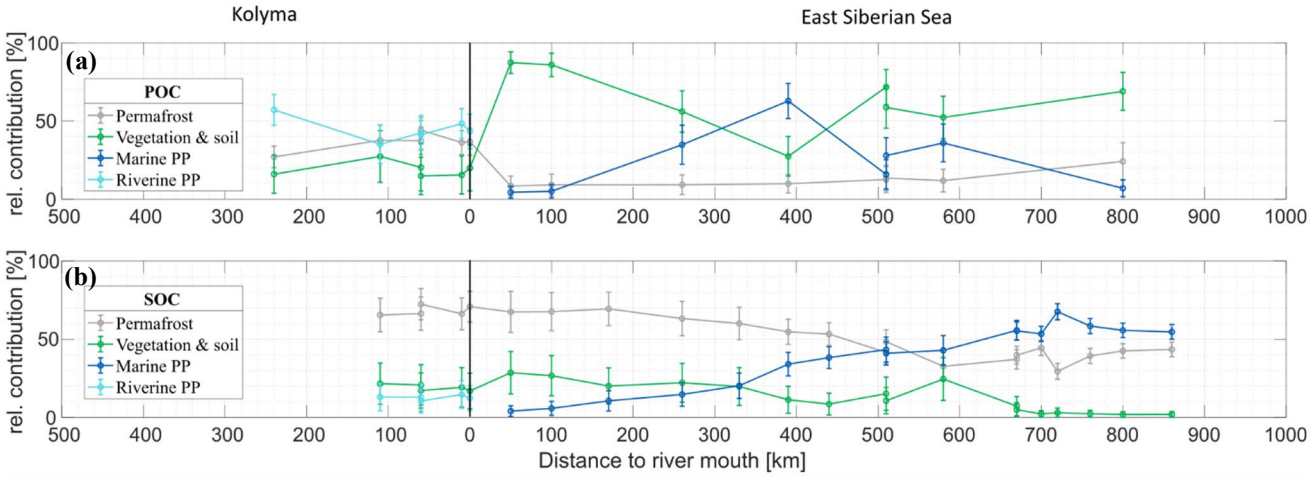

Figure A21. Mean relative contribution (plus and minus one standard deviation from Monte Carlo simulations) of three endmembers over transect distance for ~~Relative contribution of three endmembers over transect distance for~~ (a) surface water particulate organic carbon (POC) and (b) sediment organic carbon (SOC), based on dual carbon isotope ($\Delta^{14}C$ and $\delta^{13}C$) endmember analyses (EMMA). For the riverine part of the transect (Kolyma; left side of the figure), the endmembers are: Permafrost organic carbon (OC) in grey, Vegetation/soil OC in green, and Riverine primary production (PP) OC in cyan. For the marine part of the transect (East Siberian Sea; right side of the figure), the endmembers are: Permafrost OC in grey, Vegetation/soil OC in green, and Marine primary production OC in dark blue. This figure was made using the alternative Marine PP endmember ($\delta^{13}C$ = -21 ± 1‰), for comparison to Figure 4 of the main text, which uses the Marine PP endmember of -24 ± 3‰).

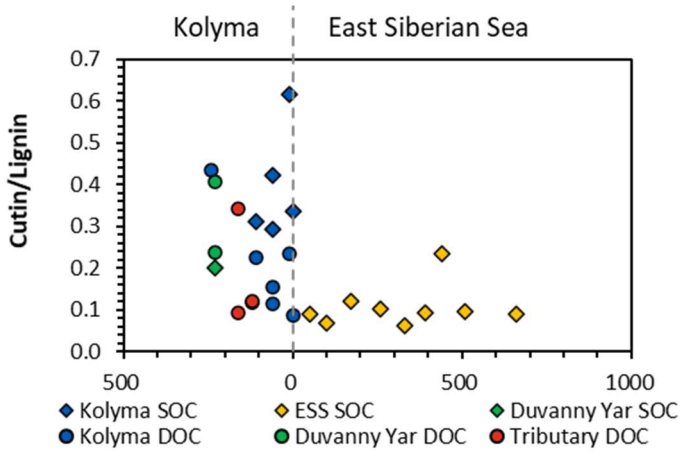

Figure A32. Cutin to Lignin ratios of Kolyma (blue), Duvanny Yar (green), tributaries (red), and East Siberian Sea (ESS; yellow) sediment organic carbon (SOC; diamonds) and dissolved organic carbon (DOC; circles).

Data availability

All data that support the findings of this study are included within the article and/or are available for download in earlier publications.

Author contributions

Conceptualisation: JEV, DJ; Formal analysis: DJ, LB, TT, PP, NH; Funding acquisition: JEV; Investigation: DJ, LB, KK, AD, NZ; Resources: TT, NZ, AD, NH, TE, JEV; Writing – original draft preparation: DJ; Writing – review & editing: all authors.

Competing interests

The authors declare that they have no conflict of interest.

Acknowledgements

This project was funded by the European Research Council as a Starting grant to J.E. Vonk (THAWSOME #676982). We want to thank the owners and staff of the Northeast Science Station (Cherskiy, Russia) for their logistical support during the field campaign. We want to thank Suzanne Verdegaal-Warmerdam, Oscar Kloostra, Martine Hagen and Roel van Elsas of the VU Amsterdam Sediment Lab and Stable Isotope Lab, and the staff of the ETH Laboratory of Ion Beam Physics for their help with the laboratory analyses.

References

Abbott, B. W., Larouche, J. R., Jones, J. B., Bowden, W. B., and Balser, A. W.: Elevated dissolved organic carbon biodegradability from thawing and collapsing permafrost, J. Geophys. Res. Biogeosciences, 119, 2049–2063, https://doi.org/10.1002/2014JG002678, 2014.

Aller, R. C. and Blair, N. E.: Carbon remineralization in the Amazon-Guianas tropical mobile mudbelt: A sedimentary incinerator, Cont. Shelf Res., 26, 2241–2259, https://doi.org/10.1016/j.csr.2006.07.016, 2006.

Alling, V., Sanchez-Garcia, L., Porcelli, D., Pugach, S., Vonk, J. E., Van Dongen, B., Mörth, C. M., Anderson, L. G., Sokolov, A., Andersson, P., Humborg, C., Semiletov, I., and Gustafsson, Ö.: Nonconservative behavior of dissolved organic carbon across the Laptev and East Siberian seas, Global Biogeochem. Cycles, 24, 1–15, https://doi.org/10.1029/2010GB003834, 2010.

Amon, R. M. W., Rinehart, A. J., Duan, S., Louchouarn, P., Prokushkin, A., Guggenberger, G., Bauch, D., Stedmon, C., Raymond, P. A., Holmes, R. M., McClelland, J. W., Peterson, B. J., Walker, S. A., and Zhulidov, A. V.: Dissolved organic matter sources in large Arctic rivers, Geochim. Cosmochim. Acta, 94, 217–237, https://doi.org/10.1016/j.gca.2012.07.015, 2012.

Andersen, J. K., Andreassen, L. M., Baker, E. H., Ballinger, T. J., Berner, L. T., Bernhard, G. H., Bhatt, U. S., Bjerke, J. W., Box, J. E., Britt, L., Brown, R., Burgess, D., Cappelen, J., Christiansen, H. H., Decharme, B., Derksen, C., Drozdov, D. S., Epstein, H. E., Farquharson, L. M., Farrell, S. L., Fausto, R. S., Fettweis, X., Fioletov, V. E., Forbes, B. C., Frost, G. V., Gerland, S., Goetz, S. J., Grooß, J.-U., Hanna, E., Hanssen-Bauer, I., Hendricks, S., Ialongo, I., Isaksen, K., Johnsen, B., Kaleschke, L., Kholodov, A. L., Kim, S.-J., Kohler, J., Labe, Z., Ladd, C., Lakkala, K., Lara, M. J., Loomis, B., Luks, B., Luojus, K., Macander, M. J., Malkova, G. V., Mankoff, K. D., Manney, G. L., Marsh, J. M., Meier, W., Moon, T. A., Mote, T., Mudryk, L., Mueter, F. J., Müller, R., Nyland, K. E., O'Neel, S., Overland, J. E., Perovich, D., Phoenix, G. K., Raynolds, M. K., Reijmer, C. H., Ricker, R., Romanovsky, V. E., Schuur, E. A. G., Sharp, M., Shiklomanov, N. I., Smeets, C. J. P. P., Smith, S. L., Streletskiy, D. A., Tedesco, M., Thoman, R. L., Thorson, J. T., Tian-Kunze, X., Timmermans, M.-L., Tømmervik, H., Tschudi, M., van As, D., van de Wal, R. S. W., Walker, D. A., Walsh, J. E., Wang, M., Webster, M., Winton, Ø., Wolken, G. J., Wood, K., Wouters, B., and Zador, S.: The Arctic, Bull. Am. Meteorol. Soc., 101, S239–S286, https://doi.org/10.1175/BAMS-D-20-0086.1, 2020.

Andersson, A.: A systematic examination of a random sampling strategy for source apportionment calculations, Sci. Total Environ., 412–413, 232–238, https://doi.org/10.1016/j.scitotenv.2011.10.031, 2011.

Andersson, A., Deng, J., Du, K., Zheng, M., Yan, C., Sköld, M., and Gustafsson, Ö.: Regionally-varying combustion sources of the january 2013 severe haze events over eastern China, Environ. Sci. Technol., 49, 2038–2043, https://doi.org/10.1021/es503855e, 2015.

Battin, T. J., Luyssaert, S., Kaplan, L. A., Aufdenkampe, A. K., Richter, A., and Tranvik, L. J.: The boundless carbon cycle, Nat. Geosci., 2, 598–600, https://doi.org/10.1038/ngeo618, 2009.

Biskaborn, B. K., Smith, S. L., Noetzli, J., Matthes, H., Vieira, G., Streletskiy, D. A., Schoeneich, P., Romanovsky, V. E., Lewkowicz, A. G., Abramov, A., Allard, M., Boike, J., Cable, W. L., Christiansen, H. H., Delaloye, R., Diekmann, B., Drozdov, D., Etzelmüller, B., Grosse, G., Guglielmin, M., Ingeman-Nielsen, T., Isaksen, K., Ishikawa, M., Johansson, M., Johannsson, H., Joo, A., Kaverin, D., Kholodov, A., Konstantinov, P., Kröger, T., Lambiel, C., Lanckman, J.-P., Luo, D., Malkova, G., Meiklejohn, I., Moskalenko, N., Oliva, M., Phillips, M., Ramos, M., Sannel, A. B. K., Sergeev, D., Seybold, C., Skryabin, P., Vasiliev, A., Wu, Q., Yoshikawa, K., Zheleznyak, M., and Lantuit, H.: Permafrost is warming at a global scale, Nat. Commun., 10, 264, https://doi.org/10.1038/s41467-018-08240-4, 2019.

Blair, N. E. and Aller, R. C.: The fate of terrestrial organic carbon in the Marine environment, Ann. Rev. Mar. Sci., 4, 401–423, https://doi.org/10.1146/annurev-marine-120709-142717, 2012.

Bosch, C., Andersson, A., Kruså, M., Bandh, C., Hovorková, I., Klánová, J., Knowles, T. D. J., Pancost, R. D., Evershed, R. P., and Gustafsson, Ö.: Source Apportionment of Polycyclic Aromatic Hydrocarbons in Central European Soils with Compound-Specific Triple Isotopes (δ 13 C, Δ 14 C, and δ 2 H), Environ. Sci. Technol., 49, 7657–7665, https://doi.org/10.1021/acs.est.5b01190, 2015.

Bröder, L., Tesi, T., Andersson, A., Eglinton, T. I., Semiletov, I. P., Dudarev, O. V., Roos, P., and Gustafsson, Ö.: Historical records of organic matter supply and degradation status in the East Siberian Sea, Org. Geochem., 91, 16–30, https://doi.org/10.1016/j.orggeochem.2015.10.008, 2016.

Bröder, L., Tesi, T., Andersson, A., Semiletov, I., and Gustafsson, Ö.: Bounding cross-shelf transport time and degradation in Siberian-Arctic land-ocean carbon transfer, Nat. Commun., 9, https://doi.org/10.1038/s41467-018-03192-1, 2018.

Bröder, L., Andersson, A., Tesi, T., Semiletov, I., and Gustafsson, Ö.: Quantifying Degradative Loss of Terrigenous Organic Carbon in Surface Sediments Across the Laptev and East Siberian Sea, Global Biogeochem. Cycles, 33, 85–99, https://doi.org/10.1029/2018GB005967, 2019.

Bröder, L., Davydova, A., Davydov, S., Zimov, N., Haghipour, N., Eglinton, T. I., and Vonk, J. E.: Particulate Organic Matter Dynamics in a Permafrost Headwater Stream and the Kolyma River Mainstem, J. Geophys. Res. Biogeosciences, 125, 1–16, https://doi.org/10.1029/2019JG005511, 2020.

Brunauer, S., Emmett, P. H., and Teller, E.: Adsorption of Gases in Multimolecular Layers, J. Am. Chem. Soc., 60, 309–319, https://doi.org/10.1021/ja01269a023, 1938.

Cole, J. J., Prairie, Y. T., Caraco, N. F., McDowell, W. H., Tranvik, L. J., Striegl, R. G., Duarte, C. M., Kortelainen, P., Downing, J. A., Middelburg, J. J., and Melack, J.: Plumbing the global carbon cycle: Integrating inland waters into the terrestrial carbon budget, 10, 171–184, https://doi.org/10.1007/s10021-006-9013-8, 2007.

Coppola, L., Gustafsson, Ö., Andersson, P., Eglinton, T. I., Uchida, M., and Dickens, A. F.: The importance of ultrafine particles as a control on the distribution of organic carbon in Washington Margin and Cascadia Basin sediments, Chem. Geol., 243, 142–156, https://doi.org/10.1016/j.chemgeo.2007.05.020, 2007.

Deirmendjian, L., Lambert, T., Morana, C., Bouillon, S., Descy, J. P., Okello, W., and Borges, A. V.: Dissolved organic matter composition and reactivity in Lake Victoria, the world's largest tropical lake, Biogeochemistry, 150, 61–83, https://doi.org/10.1007/s10533-020-00687-2, 2020.

Drake, T. W., Raymond, P. A., and Spencer, R. G. M.: Terrestrial carbon inputs to inland waters: A current synthesis of estimates and uncertainty, Limnol. Oceanogr. Lett., 3, 132–142, https://doi.org/10.1002/lol2.10055, 2018.

Dudarev, O., Charkin, A., Shakhova, N., Ruban, A., and Semiletov, I.: Progress in Oceanography East Siberian Sea : Interannual heterogeneity of the suspended particulate matter and its biogeochemical signature, 208, https://doi.org/10.1016/j.pocean.2022.102903, 2022.

Eglinton, G. and Hamilton, R. J.: Leaf Epicuticular Waxes, Science (80-.)., 156, 1322–1335, https://doi.org/10.1126/science.156.3780.1322, 1967.

Feng, X., Vonk, J. E., van Dongen, B. E., Gustafsson, O., Semiletov, I. P., Dudarev, O. V., Wang, Z., Montlucon, D. B., Wacker, L., and Eglinton, T. I.: Differential mobilization of terrestrial carbon pools in Eurasian Arctic river basins, Proc. Natl. Acad. Sci., 110, 14168–14173, https://doi.org/10.1073/pnas.1307031110, 2013.

Feng, X., Vonk, J. E., Griffin, C., Zimov, N., Montluçon, D. B., Wacker, L., and Eglinton, T. I.: 14C Variation of Dissolved Lignin in Arctic River Systems, ACS Earth Sp. Chem., 1, 334–344, https://doi.org/10.1021/acsearthspacechem.7b00055, 2017.

Freeman, K. H. and Pancost, R. D.: Biomarkers for Terrestrial Plants and Climate, in: Treatise on Geochemistry, Elsevier, 395–416, https://doi.org/10.1016/B978-0-08-095975-7.01028-7, 2014.

Freymond, C. V., Kündig, N., Stark, C., Peterse, F., Buggle, B., Lupker, M., Plötze, M., Blattmann, T. M., Filip, F., Giosan, L., and Eglinton, T. I.: Evolution of biomolecular loadings along a major river system, Geochim. Cosmochim. Acta, 223, 389–404, https://doi.org/10.1016/j.gca.2017.12.010, 2018.

Galimov, E. M., Kodina, L. A., Stepanets, O. V., and Korobeinik, G. S.: Biogeochemistry of the Russian Arctic. Kara Sea: Research results under the SIRRO project, 1995-2003, Geochemistry Int., 44, 1053–1104, https://doi.org/10.1134/S0016702906110012, 2006.

Goñi, M. A. and Hedges, J. I.: Lignin Dimers - Structures, Distribution, and Potential Geochemical Applications, Geochim. Cosmochim. Acta, 56, 4025–4043, 1992.

Goñi, M. A. and Montgomery, S.: Alkaline CuO oxidation with a microwave digestion system: Lignin analyses of geochemical samples, Anal. Chem., 72, 3116–3121, https://doi.org/10.1021/ac991316w, 2000.

Goñi, M. A., Yunker, M. B., MacDonald, R. W., and Eglinton, T. I.: Distribution and sources of organic biomarkers in arctic sediments from the Mackenzie River and Beaufort Shelf, Mar. Chem., 71, 23–51, https://doi.org/10.1016/S0304-4203(00)00037-2, 2000.

Haghipour, N., Ausin, B., Usman, M. O., Ishikawa, N., Wacker, L., Welte, C., Ueda, K., and Eglinton, T. I.: Compound-Specific Radiocarbon Analysis by Elemental Analyzer–Accelerator Mass Spectrometry: Precision and Limitations, Anal. Chem., 91, 2042–2049, https://doi.org/10.1021/acs.analchem.8b04491, 2018.

Hedges, J. I. and Mann, D. C.: The characterization of plant tissues by their lignin oxidation products, Geochim. Cosmochim. Acta, 43, 1803–1807, https://doi.org/10.1016/0016-7037(79)90028-0, 1979.

Hedges, J. I., Blanchette, R. A., Weliky, K., and Devol, A. H.: Effects of fungal degradation on the CuO oxidation products of lignin: A controlled laboratory study, Geochim. Cosmochim. Acta, 52, 2717–2726, https://doi.org/10.1016/0016-7037(88)90040-3, 1988.

Hemingway, J. D., Rothman, D. H., Grant, K. E., Rosengard, S. Z., Eglinton, T. I., Derry, L. A., and Galy, V. V.: Mineral protection regulates long-term global preservation of natural organic carbon, Nature, 570, 228–231, https://doi.org/10.1038/s41586-019-1280-6, 2019.

Hernes, P. J., Robinson, A. C., and Aufdenkampe, A. K.: Fractionation of lignin during leaching and sorption and implications for organic matter “freshness,” Geophys. Res. Lett., 34, 1–6, https://doi.org/10.1029/2007GL031017, 2007.

Hilton, R. G., Galy, V., Gaillardet, J., Dellinger, M., Bryant, C., O’Regan, M., Gröcke, D. R., Coxall, H., Bouchez, J., and Calmels, D.: Erosion of organic carbon in the Arctic as a geological carbon dioxide sink, Nature, 524, 84–87, https://doi.org/10.1038/nature14653, 2015.

Holmes, R. M., McClelland, J. W., Peterson, B. J., Tank, S. E., Bulygina, E., Eglinton, T. I., Gordeev, V. V., Gurtovaya, T. Y., Raymond, P. A., Repeta, D. J., Staples, R., Striegl, R. G., Zhulidov, A. V., and Zimov, S. A.: Seasonal and Annual Fluxes of Nutrients and Organic Matter from Large Rivers to the Arctic Ocean and Surrounding Seas, 35, 369–382, https://doi.org/10.1007/s12237-011-9386-6, 2012.

Houel, S., Louchouarn, P., Lucotte, M., Canuel, R., and Ghaleb, B.: Translocation of soil organic matter following reservoir impoundment in boreal systems: Implications for in situ productivity, Limnol. Oceanogr., 51, 1497–1513, https://doi.org/10.4319/lo.2006.51.3.1497, 2006.

Hugelius, G., Strauss, J., Zubrzycki, S., Harden, J. W., Schuur, E. A. G., Ping, C. L., Schirrmeister, L., Grosse, G., Michaelson, G. J., Koven, C. D., O'Donnell, J. A., Elberling, B., Mishra, U., Camill, P., Yu, Z., Palmtag, J., and Kuhry, P.: Estimated stocks of circumpolar permafrost carbon with quantified uncertainty ranges and identified data gaps, 11, 6573–6593, https://doi.org/10.5194/bg-11-6573-2014, 2014.

IPCC: Climate Change 2021: The Physical Science Basis. Contribution of Working Group I to the Sixth Assessment Report of the Intergovernmental Panel on Climate Change [Masson-Delmotte, V., P. Zhai, A. Pirani, S.L. Connors, C. Péan, S. Berger, N. Caud, Y. Chen, L. Goldfarb, M.I. Gomis, M. Huang, K. Leitzell, E. Lonnoy, J.B.R. Matthews, T.K. Maycock, T. Waterfield, O. Yelekçi, R. Yu, and B. Zhou (eds.)]. Cambridge University Press, Cambridge, United Kingdom and New York, NY, USA, In press, doi:10.1017/9781009157896, 2021.

Jong, D., Bröder, L., Tanski, G., Fritz, M., Lantuit, H., Tesi, T., Haghipour, N., Eglinton, T. I., and Vonk, J. E.: Nearshore zone dynamics determine pathway of organic carbon from eroding permafrost coasts, Geophys. Res. Lett., https://doi.org/10.1029/2020GL088561, 2020.

Karlsson, E. S., Charkin, A., Dudarev, O., Semiletov, I., Vonk, J. E., Sánchez-García, L., and Andersson, A.: Carbon isotopes and lipid biomarker investigation of sources, transport and degradation of terrestrial organic matter in the Buor-Khaya Bay, SE Laptev Sea, 8, 1865–1879, https://doi.org/10.5194/bg-8-1865-2011, 2011.

Keil, R. G., Montluçon, D. B., Prahl, F. G., and Hedges, J. I.: Sorptive preservation of labile organic matter in marine sediments, Nature, 370, 549–552, https://doi.org/10.1038/370549a0, 1994.

Keil, R. G., Mayer, L. M., Quay, P. D., Richey, J. E., and Hedges, J. I.: Loss of organic matter from riverine particles in deltas, Geochim. Cosmochim. Acta, 61, 1507–1511, https://doi.org/10.1016/S0016-7037(97)00044-6, 1997.

Keskitalo, K. H., Bröder, L., Jong, D., Zimov, N., Davydova, A., Davydov, S., Tesi, T., Mann, P. J., Haghipour, N., Eglinton, T. I., and Vonk, J. E.: Seasonal variability in particulate organic carbon degradation in the Kolyma River, Siberia, Environ. Res. Lett., 17, 034007, https://doi.org/10.1088/1748-9326/ac4f8d, 2022.

Kleber, M., Bourg, I. C., Coward, E. K., Hansel, C. M., Myneni, S. C. B., and Nunan, N.: Dynamic interactions at the mineral–organic matter interface, Nat. Rev. Earth Environ., 2, 402–421, https://doi.org/10.1038/s43017-021-00162-y, 2021.

Komada, T., Anderson, M. R., and Dorfmeier, C. L.: Carbonate removal from coastal sediments for the determination of organic carbon and its isotopic signatures, d13C and D14C: comparison of fumigation and direct acidification by hydrochloric acid, Limnol. Oceanogr. Methods, 6, 254–262, https://doi.org/10.4319/lom.2008.6.254, 2008.

Louchouarn, P., Opsahl, S., and Benner, R.: Isolation and Quantification of Dissolved Lignin from Natural Waters Using Solid-Phase Extraction and GC / MS, Anal. Chem., 72, 2780–2787, https://doi.org/10.1021/ac9912552, 2000.

Mann, P. J., Davydova, A., Zimov, N., Spencer, R. G. M., Davydov, S., Bulygina, E., Zimov, S., and Holmes, R. M.: Controls on the composition and lability of dissolved organic matter in Siberia's Kolyma River basin, J. Geophys. Res. Biogeosciences, 117, 1–15, https://doi.org/10.1029/2011JG001798, 2012.

Mann, P. J., Eglinton, T. I., McIntyre, C. P., Zimov, N., Davydova, A., Vonk, J. E., Holmes, R. M., and Spencer, R. G. M.: Utilization of ancient permafrost carbon in headwaters of Arctic fluvial networks, Nat. Commun., 6, 1–7, https://doi.org/10.1038/ncomms8856, 2015.

Mayer, L. M.: Surface area control of organic carbon accumulation in continental shelf sediments, Geochim. Cosmochim. Acta, 58, 1271–1284, https://doi.org/10.1016/0016-7037(94)90381-6, 1994.

McClelland, J. W., Holmes, R. M., Peterson, B. J., Raymond, P. A., Striegl, R. G., Zhulidov, A. V., Zimov, S. A., Zimov, N., Tank, S. E., Spencer, R. G. M., Staples, R., Gurtovaya, T. Y., and Griffin, C. G.: Particulate organic carbon and nitrogen export from major Arctic rivers, Global Biogeochem. Cycles, 30, https://doi.org/10.1002/2015GB005351, 2016.

McIntyre, C. P., Wacker, L., Haghipour, N., Blattmann, T. M., Fahrni, S., Usman, M., Eglinton, T. I., and Synal, H. A.: Online 13C and 14C Gas Measurements by EA-IRMS-AMS at ETH Zürich, Radiocarbon, 59, 893–903, https://doi.org/10.1017/RDC.2016.68, 2017.

Meyers, P. A.: Preservation of elemental and isotopic source identification of sedimentary organic matter, Chem. Geol., 114, 289–302, https://doi.org/10.1016/0009-2541(94)90059-0, 1994.

Neff, J. C., Finlay, J. C., Zimov, S. A., Davydov, S. P., Carrasco, J. J., Schuur, E. A. G., and Davydova, A. I.: Seasonal changes in the age and structure of dissolved organic carbon in Siberian rivers and streams, Geophys. Res. Lett., 33, 1–5, https://doi.org/10.1029/2006GL028222, 2006.

Opsahl, S. and Benner, R.: Early diagenesis of vascular plant tissues: Lignin and cutin decomposition and biogeochemical implications, Geochim. Cosmochim. Acta, 59, 4889–4904, https://doi.org/10.1016/0016-7037(95)00348-7, 1995.

Repasch, M., Scheingross, J. S., Hovius, N., Lupker, M., Wittmann, H., Haghipour, N., Gröcke, D. R., Orfeo, O., Eglinton, T. I., and Sachse, D.: Fluvial organic carbon cycling regulated by sediment transit time and mineral protection, Nat. Geosci., 14, 842–848, https://doi.org/10.1038/s41561-021-00845-7, 2021.

Rogers, J. A., Galy, V., Kellerman, A. M., Chanton, J. P., Zimov, N., and Spencer, R. G. M.: Limited Presence of Permafrost Dissolved Organic Matter in the Kolyma River, Siberia Revealed by Ramped Oxidation, J. Geophys. Res. Biogeosciences, 126, 1–18, https://doi.org/10.1029/2020JG005977, 2021.

Salvadó, J. A., Tesi, T., Sundbom, M., Karlsson, E., Krusä, M., Semiletov, I. P., Panova, E., and Gustafsson, Ö.: Contrasting composition of terrigenous organic matter in the dissolved, particulate and sedimentary organic carbon pools on the outer East Siberian Arctic Shelf, 13, 6121–6138, https://doi.org/10.5194/bg-13-6121-2016, 2016.

Sánchez-García, L., Vonk, J. E., Charkin, A. N., Kosmach, D., Dudarev, O. V., Semiletov, I. P., and Gustafsson, O.: Characterisation of three regimes of collapsing arctic ice complex deposits on the SE Laptev Sea coast using biomarkers and dual carbon isotopes, Permafr. Periglac. Process., 25, 172–183, https://doi.org/10.1002/ppp.1815, 2014.

Scheingross, J. S., Hovius, N., Dellinger, M., Hilton, R. G., Repasch, M., Sachse, D., Gröcke, D. R., Vieth-Hillebrand, A., and Turowski, J. M.: Preservation of organic carbon during active fluvial transport and particle abrasion, Geology, 47, 958–962, https://doi.org/10.1130/G46442.1, 2019.

Schuur, E. A. G., McGuire, A. D., Schädel, C., Grosse, G., Harden, J. W., Hayes, D. J., Hugelius, G., Koven, C. D., Kuhry, P., Lawrence, D. M., Natali, S. M., Olefeldt, D., Romanovsky, V. E., Schaefer, K., Turetsky, M. R., Treat, C. C., and Vonk, J. E.: Climate change and the permafrost carbon feedback, Nature, 520, 171–179, https://doi.org/10.1038/nature14338, 2015.

Semiletov, I., Pipko, I., Gustafsson, Ö., Anderson, L. G., Sergienko, V., Pugach, S., Dudarev, O., Charkin, A., Gukov, A., Bröder, L., Andersson, A., Spivak, E., and Shakhova, N.: Acidification of East Siberian Arctic Shelf waters through addition of freshwater and terrestrial carbon, 9, https://doi.org/10.1038/NEGO2695, 2016.

Shakil, S., Tank, S. E., Kokelj, S. V., Vonk, J. E., and Zolkos, S.: Particulate dominance of organic carbon mobilization from thaw slumps on the Peel Plateau, NT: Quantification and implications for stream systems and permafrost carbon release, Environ. Res. Lett., https://doi.org/10.1088/1748-9326/abac36, 2020.

Shiklomanov, A.I., R.M. Holmes, J.W. McClelland, S.E. Tank, and R.G.M. Spencer: Arctic Great Rivers Observatory. Discharge Dataset, Version 20220630, 2021.

Spencer, R. G. M., Aiken, G. R., Dyda, R. Y., Butler, K. D., Bergamaschi, B. A., and Hernes, P. J.: Comparison of XAD with other dissolved lignin isolation techniques and a compilation of analytical improvements for the analysis of lignin in aquatic settings, Org. Geochem., 41, 445–453, https://doi.org/10.1016/J.ORGGEOCHEM.2010.02.004, 2010.

Stein, R., Macdonald, R.W. (Eds.), The Organic Carbon Cycle in the Arctic Ocean. Springer Verlag, 2004.

Stuiver, M. and Polach, H. A.: Discussion Reporting of 14 C Data, Radiocarbon, 19, 355–363, https://doi.org/10.1017/S0033822200003672, 1977.

Terhaar, J., Lauerwald, R., Regnier, P., Gruber, N., and Bopp, L.: Around one third of current Arctic Ocean primary production sustained by rivers and coastal erosion, Nat. Commun., 12, https://doi.org/10.1038/s41467-020-20470-z, 2021.

Tesi, T., Semiletov, I., Hugelius, G., Dudarev, O., Kuhry, P., and Gustafsson, Ö.: Composition and fate of terrigenous organic matter along the Arctic land-ocean continuum in East Siberia: Insights from biomarkers and carbon isotopes, Geochim. Cosmochim. Acta, 133, 235–256, https://doi.org/10.1016/j.gca.2014.02.045, 2014.

Tesi, T., Semiletov, I., Dudarev, O., Andersson, A., and Gustafsson, Ö.: Matrix association effects on hydrodynamic sorting and degradation of terrestrial organic matter during cross-shelf transport in the Laptev and East Siberian shelf seas, J. Geophys. Res. Biogeosciences, 121, 731–752, https://doi.org/10.1002/2015JG003067, 2016.

Vonk, J. E., Sánchez-García, L., Semiletov, I., Dudarev, O., Eglinton, T., Andersson, A., and Gustafsson, O.: Molecular and radiocarbon constraints on sources and degradation of terrestrial organic carbon along the Kolyma paleoriver transect, East Siberian Sea, 7, 3153–3166, https://doi.org/10.5194/bg-7-3153-2010, 2010a.

Vonk, J. E., Van Dongen, B. E., and Gustafsson, Ö.: Selective preservation of old organic carbon fluvially released from sub-Arctic soils, Geophys. Res. Lett., 37, 5–9, https://doi.org/10.1029/2010GL042909, 2010b.

Vonk, J. E., Sánchez-García, L., van Dongen, B. E., Alling, V., Kosmach, D., Charkin, A., Semiletov, I. P., Dudarev, O. V., Shakhova, N., Roos, P., Eglinton, T. I., Andersson, A., and Gustafsson, Ö.: Activation of old carbon by erosion of coastal and subsea permafrost in Arctic Siberia, Nature, 489, 137–140, https://doi.org/10.1038/nature11392, 2012.

Vonk, J. E., Mann, P. J., Davydov, S., Davydova, A., Spencer, R. G. M., Schade, J., Sobczak, W. V., Zimov, N., Zimov, S., Bulygina, E., Eglinton, T. I., and Holmes, R. M.: High biolability of ancient permafrost carbon upon thaw, Geophys. Res. Lett., 40, 2689–2693, https://doi.org/10.1002/grl.50348, 2013.

Vonk, J. E., Tank, S. E., Bowden, W. B., Laurion, I., Vincent, W. F., Alekseychik, P., Amyot, M., Billet, M. F., Canário, J., Cory, R. M., Deshpande, B. N., Helbig, M., Jammet, M., Karlsson, J., Larouche, J., MacMillan, G., Rautio, M., Walter Anthony, K. M., and Wickland, K. P.: Reviews and Syntheses: Effects of permafrost thaw on arctic aquatic ecosystems, https://doi.org/10.5194/bgd-12-10719-2015, 2015.

Wakeham, S. G., Canuel, E. A., Lerberg, E. J., Mason, P., Sampere, T. P., and Bianchi, T. S.: Partitioning of organic matter in continental margin sediments among density fractions, Mar. Chem., 115, 211–225, https://doi.org/10.1016/j.marchem.2009.08.005, 2009.

Walvoord, M. A. and Kurylyk, B. L.: Hydrologic Impacts of Thawing Permafrost-A Review, Vadose Zo. J., 15, vzj2016.01.0010, https://doi.org/10.2136/vzj2016.01.0010, 2016.

Wild, B., Andersson, A., Bröder, L., Vonk, J., Hugelius, G., McClelland, J. W., Song, W., Raymond, P. A., and Gustafsson, Ö.: Rivers across the Siberian Arctic unearth the patterns of carbon release from thawing permafrost, Proc. Natl. Acad. Sci. U. S. A., 116, 10280–10285, https://doi.org/10.1073/pnas.1811797116, 2019.

Winterfeld, M., Goñi, M. A., Just, J., Hefter, J., and Mollenhauer, G.: Characterization of particulate organic matter in the Lena River delta and adjacent nearshore zone, NE Siberia - Part 2: Lignin-derived phenol compositions, 12, 2261–2283, https://doi.org/10.5194/bg-12-2261-2015, 2015a.

Winterfeld, M., Laepple, T., and Mollenhauer, G.: Characterization of particulate organic matter in the Lena River delta and adjacent nearshore zone, NE Siberia - Part I: Radiocarbon inventories, 12, 3769–3788, https://doi.org/10.5194/bg-12-3769-2015, 2015b.

Zimov, S. A., Davydov, S. P., Zimova, G. M., Davydova, A. I., Schuur, E. A. G., Dutta, K., and Chapin, I. S.: Permafrost carbon: Stock and decomposability of a globally significant carbon pool, Geophys. Res. Lett., 33, 1–5, https://doi.org/10.1029/2006GL027484, 2006a.

Zimov, S. A, Schuur, E. A. G., and Chapin, F. S.: Permafrost and the Global Carbon Budget, Science (80-.)., 312, 1612–1613, https://doi.org/10.1126/science.1128908, 2006b.